DYNAMIC FOUR-STREAM MODEL FOR POLARIZATION

By

ZEYNEP GUNAY

Bachelor of Science

Ege University

Izmir, Turkey

1998

Submitted to the Faculty of the
Graduate College of the
Oklahoma State University
in partial fulfillment of
the requirements for
the Degree of
MASTER OF SCIENCE
December, 2002

DYNAMIC FOUR-STREAM MODEL FOR

POLARIZATION

Thesis Approved:

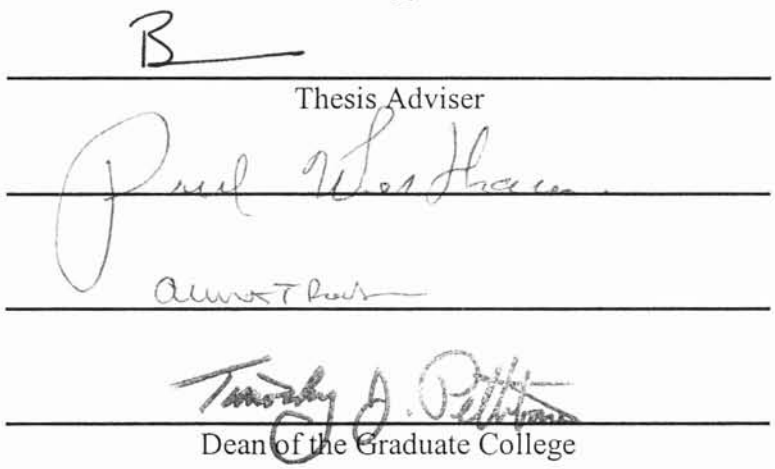

Thesis Adviser

Dean of the Graduate College

ACKNOWLEDGMENTS

I would like to express my gratitude to my advisor Dr. Bruce Ackerson for his guidance, his efforts to explain things, clearly and simply throughout this thesis. I have learned various things from him, such as, the way of thinking and the way of proceeding in theoretical research. I am sincerely grateful to Dr. R.J. Hauenstein for his help with Linux System. I especially wish to express my appreciation to Dr. P. Westhaus and Dr. A. Rosenberger for being on my committee, and reviewing my thesis. I would like to extend my gratitude to all my professors, from whom I have benefited.

I am grateful to all my friends from OSU, for being the surrogate family during the years I stayed here.

I would also like to thank my parents, Yilmaz and Tulin Gunay for their love, continued emotional support and encouragement when it was most required.

Finally, I would like to thank the Department of Physics for supporting me during these three years of study.

TABLE OF CONTENTS

LIST OF FIGURES

LIST OF TABLES

List of Symbols

Symbol	Meaning
λ	Wavelength of light in the medium
k	Wavenumber
k_0	Wavenumber of the incident light
c	Light velocity
l^*	Transport mean free path, i.e., the average distance in which light changes direction of propagation, see Eq.1.2.20
l_s	Scattering mean free path, i.e., the average distance between scattering events
l_a	Absorption length
κ	Dimensionless absorption factor, see Eq.3.4
zp	Penetration depth ratio, the distance that the photons penetrate the medium before being scattered or absorbed
zp^+	Distances greater than zp
zp^-	Distances less than zp
z_p	Scaled optical thickness, defined by $z_p = zp/(z_0(1-g))$
z_e	Extrapolation depth ratio, refer to pg.10
z_0	Dimensionality parameter, refer to pg. 16 and pg. 33
p	The fraction of photons, which go into the forward direction
R	Boundary reflectivity
$R_w(\mu)$	Angle dependent reflectivity, see Eq.1.2.17
z	z direction
z	Length element in a slab
L	Thickness of the sample
$\widetilde{L}$	Dimensionless optical thickness, defined by $L/l^* = L/(l_s z_0(1g))$
$\widetilde{h}$	Scaled optical thickness, defined by $\widetilde{L}/(z_0(1-g)) = L/l_s$
h^*	$\widetilde{h}(1-g) = L(1-g)/l_s$
t	Time variable
Δt	Time interval
τ	Delay time that represents the time between the original and the shifted signal in a correlation averaged signal

τ_0	$1/D_B k_0^{\,2}$
μ	Cosine of a scattering angle
σ	The probability that a given polarization survives in a scattering event, defined by Eq.2.2.1.a.
g	Scalar asymmetry parameter, i.e., the mean cosine of the total scattered intensity independent of state of polarization averaged over all scattering angles defined by Eq.2.2.1.b
g_c	Polarization difference asymmetry parameter, i.e, mean cosine of the polarization difference intensities averaged over all scattering angles defined by Eq.2.2.1.c
β	Efficiency of the photon collection system, signal to noise factor
q_n	Scattering wave vector after the n^{th} scattering event
$P(s)$	Fraction of photons that travel a path having length $s = nl_s$
D_B	Diffusion coefficient
U	Photon energy density
E	Electric field
$E^{(n)}$	Scattered electric filed from the n^{th} path
$\Delta\phi^{(n)}$	Phase change of an electric field due to n scatterers
$r_n(t)$	Position of the n^{th} scattering event at time t
$G_1(\tau)$	Unnormalized electric filed autocorrelation function
$g_1(\tau)$	Normalized electric field autocorrelation function
$G_T(x)$	Unnormalized transmission electric autocorrelation function
$g_T(x)$	Normalized transmission electric autocorrelation function
$G_B(x)$	Unnormalized backscattering electric autocorrelation function
$g_B(x)$	Normalized backscattering electric autocorrelation function
$g_{T_{ip}}(x)$	Normalized electric autocorrelation function for total transmitted intensity independent of polarization
$g_{T_{dp}}(x)$	Normalized electric autocorrelation function for degree of polarization in the downward direction
$T(s)$	Laplace transform of transmitted pulse
$T'(C,D,R,x_0,y_0,\widetilde{h},\lambda,s)$	Transmitted pulse after integration over all possible penetration depths is taken
T_{ip}	Total transmitted intensity independent of polarization
T_{dp}	Degree of polarization in the downward direction
T_p	Static transmission probability
T_p'	Static transmission probability after integration over all possible penetration depths is taken
$B(s)$	Laplace transform of backscattered pulse

$B'(C,D,R,x_0,y_0,\lambda,s)$	Backscattered pulse after integration over all possible penetration depths in taken
B_{ip}	Total backscattered intensity independent of polarization
B_{dp}	Degree of polarization in the upward direction
γ	The initial slope of the graph where $\lvert g_B(x)\rvert^2$ is plotted logarithmically as a function of $\sqrt{x}$, see Eq.4.2
γ_+	γ value for positive helicity channel
γ_-	γ value for opposite helicity channel
$\gamma_\parallel$	γ value for parallel polarization channel
$\gamma_\perp$	γ value for perpendicular polarization channel
δ	Polarization parameter, refer to pg. 42
I	Light intensity
I_0	Incident light intensity
$I_s(\theta)$	Scattered intensity at an angle θ
I_s	Total scattered intensity
$\bar{I}$	Laplace transform of intensity
I_d	Light intensity in downward direction
I_u	Light intensity in upward direction
I_{dp}	Light intensity in downward direction with positive polarization
I_{dm}	Light intensity in downward direction with negative polarization
I_{up}	Light intensity in the upward direction with positive polarization
I_{um}	Light intensity in the upward direction with negative polarization
$\bar{I}\downarrow_{less}(z,s)$	Laplace transform of either total downward intensity independent of polarization or degree of polarization in downward direction for $z < z_p$
$\bar{I}\downarrow_{greater}(z,s)$	Laplace transform of either total downward intensity independent of polarization or degree of polarization in downward direction for $z > z_p$
$\bar{I}\uparrow_{less}(z,s)$	Laplace transform of either total upward intensity independent of polarization or degree of polarization in upward direction for $z < z_p$
$\bar{I}\uparrow_{greater}(z,s)$	Laplace transform of either total upward intensity independent of polarization or degree of polarization in upward direction for $z > z_p$
i	Transformed intensity at the end of taking the Laplace transform with respect to time and Fourier transform with respect to space
$\mathrm{i}_{\mathrm{total}}$	Transformed total intensity in dependent of direction and polarization
$\mathrm{i}_{\mathrm{polplus}}$	Transformed intensity that shows the degree of polarization independent of propagation direction
$\mathrm{i}_{\mathrm{diff}}$	Transformed intensity that shows the net direction of propagation independent of polarization

$i_{polminus}$	Transformed intensity that shows both the net direction of propagation and degree of polarization
p_{dupm}	Transition probability that a photon directed downward with positive polarization is scattered upward with negative polarization, for other 15 probability transitions see table.1
P	Degree of polarization, see Eq.4.1
ω	Laplace time variable in two-stream theory
s	Laplace time variable in four flux theory
α	$=\sqrt{\omega(\omega+1/z_0)}$, refer to pg.21
λ_1	$=\sqrt{(s-g+\kappa+1)(s+\kappa)}$, refer to pg.37
λ_2	$=\sqrt{(s+1-g_c+\kappa)(s-2\sigma+2+\kappa)}$, refer to pg.37
λ_{20}	$=\sqrt{2(\sigma-1)(g_c-1)}$, refer to pg. 65
x	$6\tau/\tau_0$ where τ_0 represents $1/D_B k_0^{\,2}$, also see Eq.3.11
$\bar{x}$	Refer to Eq.3.1.15.a
$\bar{y}$	Refer to Eq.3.15.b
x_0	Refer to Eq.3.1.15.a
y_0	Refer to Eq.3.1.15.b
x_{less}	Refer to Eq.3.1.16.a
$x_{greater}$	Refer to Eq.3.17.a
y_{less}	Refer to Eq.3.1.16.b
$y_{greater}$	Refer to Eq.3.1.17.b
A	See Eq.1.3.14
A'	See Eq.3.2.3
B	See Eq.1.3.14
B'	See Eq.3.2.3
C	Refer to pg. 37
D	Refer to pg. 37
A_1	Refer to pg.21
A_2	Refer to pg.21
C_1	Refer to pg. 37
C_2	Refer to pg. 37

Chapter 1

Introduction

1.1 General comments on multiple scattering

When light shines on a large collection of small particles suspended in a medium, the scattering by particles diffuses the incident radiation in all directions. This is known as multiple light scattering and it gives rise to many observable phenomena, from the color of sky, brightness of clouds to darkening of sand upon wetting [1]. These are all examples of static light scattering since the time-averaged intensity of scattered light is observed. A radiative transfer equation has been derived many times from multiple scattering theory [2-7] and has been used widely in analyzing static scattering problems in stellar and planetary atmospheres, underwater and atmospheric imaging, and climatology.

More recently, dynamic light scattering, DLS, where time dependent intensity fluctuations are measured in highly multiple scattering limits, has been examined both theoretically and experimentally [8-12]. The intensity fluctuations in the scattered light occur due to the Brownian motion of the disperse particles in the medium which gives rise to a Doppler effect. So, the scattered light possesses a range of frequencies shifted slightly from the frequency of the incident light. That's why dynamic light scattering is also named quasi-elastic light scattering, QELS. The data from light scattering experiments in the weakly scattering sample can be analyzed to determine properties of

the suspended particles in the medium like the diffusion coefficient, scattering coefficient, asymmetry factor, average size of disperse particles, or viscosity [13,14]. The technique of measuring time dependent variations of the scattered light from an optically dense medium requires reinterpretation of the scattering function and is called diffusing wave spectroscopy, DWS. This technique has been applied to a wide variety of systems like gels[15], colloidal dispersions[16,17],liquid crystals [18,19],polymers[20,21]. DWS has also found its applications in biophysics in microrheology [22], imaging and studying biological tissues [23-26], especially to differentiate between tumorigenic and nontumorigenic cells. Recently, Page Cowan and Weitz applied DWS to ultrasonic waves [27].

1.2 Diffusing Wave Spectroscopy – DWS

1.2.a Theory

Fluctuations in the intensity of the multiply scattered light are measured and expressed in terms of a normalized electric field autocorrelation function. The dependence of the autocorrelation functions on the experimental geometry provides a powerful means of exploring the dynamical structural properties of the scattering medium over vastly different length and time scales [28-32]. DWS extends the single scattering technique of dynamic light scattering to the multiple scattering regimes by modeling the transport of light as a random walk between scatterers. DWS uses the diffusion approximation. This approximation assumes that the propagation of light in the medium is diffusive.

The DWS setup is shown schematically in figure 1. Here, a beam of laser light is

directed through an optically dense medium composed of particles undergoing Brownian motion. When a photon migrates through the medium, it scatters many times due to the interaction with the particles. The intensity interference produced by transmitted photons is composed of many bright and dark regions called speckles. Since the scatterers in the medium are moving, the speckle pattern fluctuates in time. DWS measurements are made over an angular area of a typical speckle using an aperture and a photomultiplier. In a way, photomultiplier collects the scattered electric field.

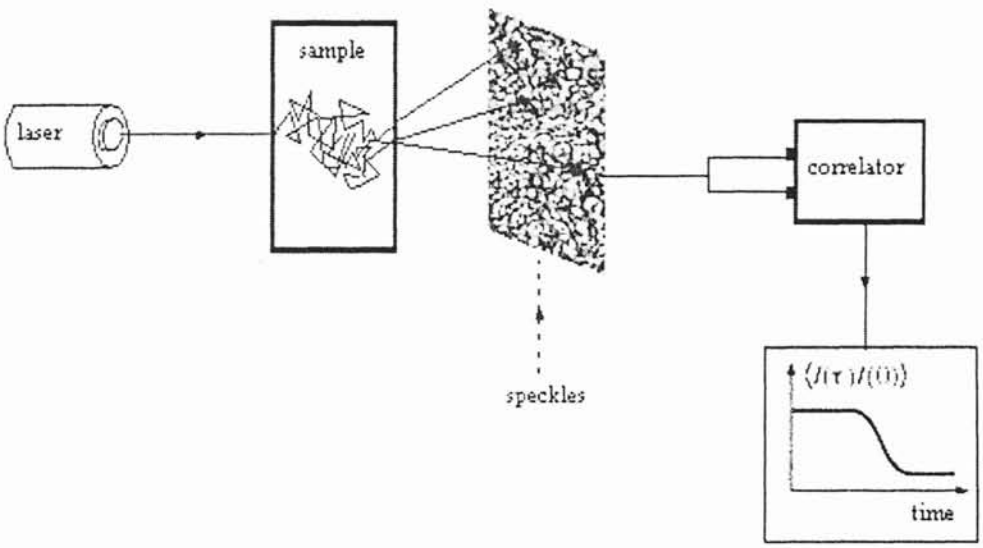

Fig.1- Schematic representation of the experiment. Laser light incident on a sample of thickness L is multiply scattered. Light is collected in a region, the size of a typical speckle and sent to a photomultiplier tube (PMT). Correlation vs. time is obtained from a correlator that is connected to PMT.

The most convenient measure of the dynamics of the scattered light is the temporal autocorrelation function of the intensity. The intensity autocorrelation function is the convolution of the intensity signal with itself at a later time, τ. The relation between the normalized intensity correlation function and the normalized electric field correlation function is given by the Siegert relation [28,32,33]. Normalized electric field autocorrelation function is defined as

$$g_1(\tau) = \frac{\langle E(0)E^*(\tau)\rangle}{\langle |E|^2 \rangle} \tag{1.2.1}$$

where $\langle\ \rangle$ denotes the average over time, t. The shift time, τ, represents the delay between the 'original' and the 'shifted' signal and is generally referred to as the delay time. The Siegert relation is given as

$$\frac{\langle I(\tau)I(0)\rangle}{\langle I\rangle^2} = 1 + \beta|g_1(\tau)|^2 \tag{1.2.2}$$

where, β, the efficiency of the photon collection system or signal to noise factor, is generally less than one. It depends on the number of speckles spanned by the detector and the stability of the laser.

In the diffusion approximation, the path of an individual photon may be pictured as a trajectory composed of straight-line segments. The average length of each line segment is named the transport mean free path, l^*, or random-walk step of photons before significant change in direction. Another characteristic length is the scattering mean free path, $l_s \leq l^*$, which is the average distance between actual scattering events. These

scattering events occur at positions $r_1(t), r_2(t), ..., r_i(t) ..., r_n(t)$ for which the scattering wave vectors are $q_1, q_2, ..., q_i, ..., q_n$. The change in position of the i^{th} particle in a time τ is written as $\Delta r_i(\tau) = r_i(\tau) - r_i(0)$.

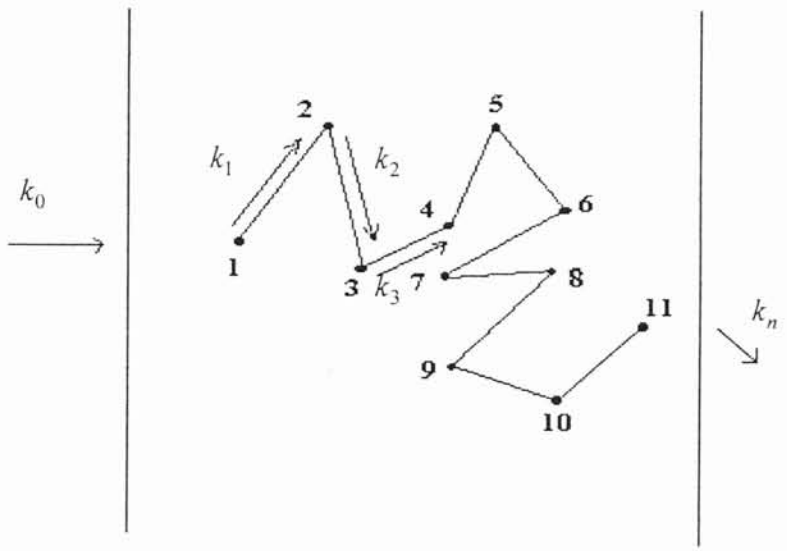

Fig.2- Schematic representation of the change in the direction of scattering vectors.

The scattering wave vector is the difference between the incident photon wave vector and the scattering wave vector, thus for multiple scattering

$$\begin{aligned} q_1 &= k_1 - k_0 \\ q_2 &= k_2 - k_1 \\ q_3 &= k_3 - k_2 \\ &\vdots \\ q_n &= k_n - k_{n-1} \\ \textstyle\sum_i q_i &= k_n - k_0 \end{aligned} \qquad (1.2.3)$$

the sum of the intermediate scattering vectors must be equal to the difference between the incident and the scattering vectors, $\sum_i q_i = k_n - k_0$. For large n, a path of n steps has

length $s = nl_s$. The contribution of a path of n scattering events to the decay of the autocorrelation function is given by

$$G_1^{(n)}(\tau) = \left\langle E^{(n)*}(0)E^{(n)}(\tau)\right\rangle = \left\langle \left|E^{(n)}(0)\right|^2 \right\rangle e^{-i\Delta\phi^{(n)}(\tau)} \tag{1.2.4}$$

where $E^{(n)}$ is the scattered electric field from the n^{th} path with $\Delta\phi^{(n)}(\tau)$ the phase change of the field due to all n scatterers where

$$\Delta\phi^{(n)}(\tau) = \sum_{i=1}^{n} q_i \Delta r_i(\tau) \tag{1.2.5}$$

When the particles in the sample move, the phase of the scattered light fluctuates. It goes through one complete cycle when the path length changes by the light wavelength, λ. With the approximation that the particles are uncorrelated and the scattering is random, the following equation can be written for the average contribution of all paths of n scatterings,

$$G_1^{(n)}(\tau) = I_s P(n)\left\langle \prod_{i=1}^{n} e^{iq_i \Delta r_i(\tau)} \right\rangle \tag{1.2.6}$$

Here, I_s is the total scattered intensity and $P(n)$ is the fraction of photons that travel a path having $n = s/l_s$ scatterings. The longer paths (larger n) contribute more to the decay of the autocorrelation function, because they generally represent larger path length changes. Uncorrelated scattering events correspond to a random distribution of q_i and a Gaussian distribution for $\Delta r(\tau)$. The average of the square of the change in positions is given as $\left\langle \Delta r^2(\tau)\right\rangle = 6D_B\tau$ where D_B is the particle Brownian diffusion coefficient. Now, Eq.1.2.4 can be written as

$$G_1^{(n)}(\tau) = I_s P(n) \left\langle e^{-q_i^2 \langle \Delta r^2(\tau) \rangle / 6} \right\rangle_q^n \tag{1.2.7}$$

where $\langle\ \rangle_q$ denotes the average over q. For isotropic scattering, $l^* = l_s$, the mean-square transfer[8] is

$$\langle q^2 \rangle = 2k_0^{\ 2} = 2\left(\frac{2\pi}{\lambda}\right)^2 \tag{1.2.8}$$

which gives

$$G_1^{(n)}(\tau) = I_s P(n) e^{-(2\tau/\tau_0)n} \tag{1.2.9}$$

where $\tau_0 = 1/D_B k_0^2$. For large n, $G_1^{(n)}(\tau)$ decays rapidly to zero. In the case of anisotropic scattering, $l^* > l_s$, the scattering intensity is peaked in the forward direction for single scattering particles making the sample. Therefore, more scattering events are required to randomize the direction of propagation. A complete randomization of the wave occurs at transport mean free path l^* [2,34,35],

$$l^* = \frac{l_s}{1 - \langle \mu \rangle}, \tag{1.2.10}$$

which gives the relation between transport mean free path and the scattering mean free path, where $\langle \mu \rangle = \langle Cos\theta \rangle$ stands for the average cosine of the scattering angle between successive scatterers. In the case of anisotropic scattering [8], the average of the square scattering wave is reduced as,

$$\langle q^2 \rangle = 2k_0^{\ 2}(l_s / l^*) \tag{1.2.11}$$

Using this, the contribution of the paths of order n is written as in Eq.1.2.12

$$G_1^{(n)}(\tau) = I_s P(n) e^{-(2\tau/\tau_0)\frac{l_s}{l^*}n} \tag{1.2.12}$$

The contributions of all paths are calculated to obtain the time correlation function. Summing over scattering paths of all orders yields

$$G_1(\tau) = I_s \sum_{n=1}^{\infty} P(n) e^{-(2\tau/\tau_0)\frac{l_s}{l^*}n} \tag{1.2.13}$$

$G_1(\tau)$ is called the total autocorrelation function. It is more clear in Eq.1.2.13 that decay rate of a given path depends on its length. There are so many scatterers on a long path that each particle must move only a fraction of a wavelength for the phase to change by π. This leads to a rapid decay rate. On a short path each particle must move a substantial distance for a phase change of π. This leads to a slower decay rate. Summation over n is approximated as the integral over the path length s.

$$G_1(\tau) = I_s \int P(s) e^{-(2\tau/\tau_0)s/l^*} ds = I_s \int P(s) e^{-xs/(3l^*)} ds \tag{1.2.14}$$

Here, $x = 2k_0{}^2 \left\langle \Delta r^2(\tau) \right\rangle = \dfrac{6\tau}{\tau_0}$

$G_1(\tau)$ becomes the Laplace transform of $P(s)$ when the limits of integration in Eq.1.2.14 are extended from $s = 0$ to $s = \infty$. Thus, the autocorrelation function can be obtained by solving the Laplace transform of the Diffusion equation.

1.2.b Transmission:

For the transport geometry, consider a slab of thickness L and infinite lateral extent to be illuminated by a pulse of light [32]. The multiple scattered photons are detected at a point r on the other side of slab. The change of the intensity at r is shown in figure 3. The intensity of light at point r increases to maximum as the light diffuses through, then decreases to zero when all photons have left the sample. At time t, the photons arriving at r are the ones that have traveled a distance of $s = ct$. Since $P(s)$ is the fraction of photons that have migrated a path of length s, it is also the number of photons that have been in the sample at time t. The most convenient way to obtain $P(s)$ for transmission is to solve the diffusion equation with the appropriate boundary conditions [2].

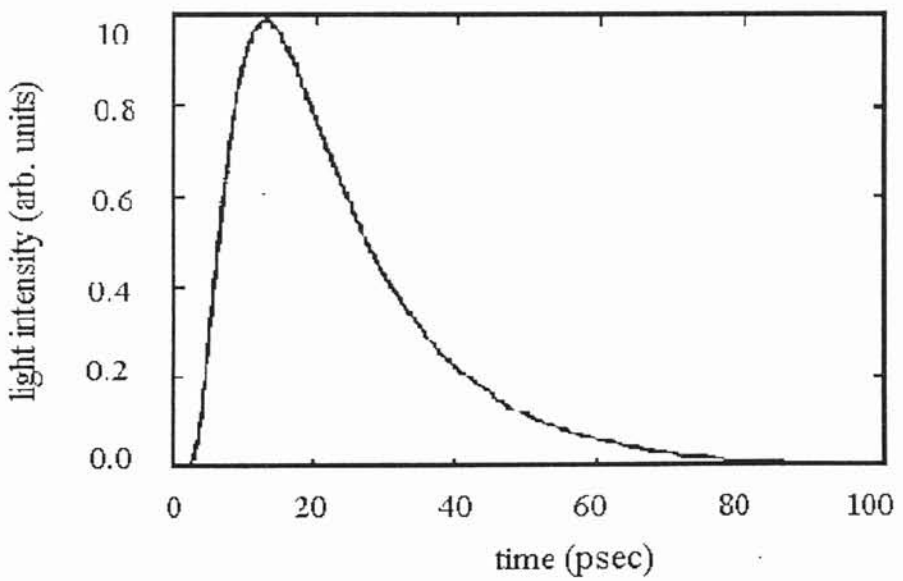

Fig.3- The dependence of the detected transmission intensity of an incident delta function pulse sent on a sample with $L = 1mm$ and $l^* = 100\mu m$.

The diffusion equation is given by

$$\frac{\partial U(r,r_0,t)}{\partial t} = D_B \nabla^2 U \tag{1.2.15}$$

where a measurable macroscopic observable, $U(r,r_0,t)$, is the photon energy density within the sample. The dependence of the diffusion coefficient on l^* is assumed to be $D_B = cl^*/3$ where c is the speed of light in the medium. The flux of the diffusing photons detected on the boundary at r is given by the normal derivative of U and is assumed proportional to the probability P(s) by these authors [8].

$$P(s) \propto \hat{n}.\nabla U\big|_r$$

where $\hat{n}$ denotes the unit normal vector, directed outward. Plugging $P(s)$ found from diffusion equation into Eq.1.2.14 gives Eq.1.2.16 for correlation function for the transmission geometry under consideration. However, taking the lower limit of integration as 0 allows unphysical short paths to contribute to the correlation function. Therefore, this approach is good only for long paths in a transmission measurement.

$$G_T(x) = \frac{Sinh(zp\sqrt{x}) + z_e\sqrt{x}Cosh(zp\sqrt{x})}{(1+z_e{}^2x)Sinh(\widetilde{L}\sqrt{x}) + 2z_e\sqrt{x}Cosh(\widetilde{L}\sqrt{x})} \tag{1.2.16}$$

Here, $\widetilde{L} = L/l^*$ is the dimensionless optical thickness. The penetration depth ratio and the extrapolation depth ratio are shown by zp and z_e respectively [37-39]. They are both in the solution of the diffusion equation and are of order one. The concentration field U extrapolates to zero at $z_e l^*$. The extrapolation depth ratio is specified by the angle dependent reflectivity, $R_w(\mu)$ [36].

$$z_e = \frac{2}{3}\left(\frac{1+R_2}{1-R_1}\right) \text{ with } R_n = \int_0^1 (n+1)\mu^n R_w(\mu)d\mu \tag{1.2.17}$$

Accurate calculation of z_e for unknown boundary conditions from the angular dependence of the diffuse transmission has been discussed by Durian [37-39]. To get the normalized transmission correlation function Eq.1.2.16 should be divided by the static diffuse transition probability T_p [10].

$$T_p = \frac{zp + z_e}{\widetilde{L} + 2z_e} = G_T(0) \tag{1.2.18}$$

The penetration depth ratio depends on scattering length and mostly is taken to be $zp = 1$. If the scattering is isotropic, the photons are randomized immediately upon multiple scattering. For anisotropic scattering events photons are not randomized immediately, since the photons scatter preferentially in the forward direction. A better approximation results when averaging over the deposition depth zp weighted by Beer's law.

$$T_p' = \int_0^{\widetilde{L}} T_p e^{-zpl^*/l_s} l^*/l_s dzp = \frac{(1+z_e) - (1+z_e+\widetilde{L})e^{-L/l_s}}{\widetilde{L} + 2z_e} \tag{1.2.19}$$

The exponential term in the integral corresponds to the attenuation decay of the incident beam source with depth. The transmission correlation function found in Eq.1.2.16 should be divided by Eq.1.2.19 after the average over zp is taken in order to get the normalized correlation function.

$$g_T(x) = \frac{(1+z_e)\sqrt{x} - [(1+z_e x)Sinh\widetilde{L}\sqrt{x} + (1+z_e)\sqrt{x}Cosh\widetilde{L}\sqrt{x}]e^{-\widetilde{L}}}{T_p'(1-x)[(1+z_e^2 x)Sinh\widetilde{L}\sqrt{x} + 2z_e\sqrt{x}Cosh\widetilde{L}\sqrt{x}]} \tag{1.2.20}$$

The decay is nearly exponential in $(L/l^*)^2 x$. The coefficient of x shows the mean numbers of steps for a random walk taken by a transmitted photon. The length $(L/l^*)^2 l^*$ is generally called the characteristic path length and is directly reflected in the autocorrelation function as a characteristic decay time [8]. The characteristic path length changes by $\sim \lambda$ during one characteristic decay time. This corresponds to a total phase change of π.

$$\left\langle (\Delta\phi)^2 \right\rangle \approx \left(\frac{L}{l^*}\right)^2 \frac{l^*}{l} \left\langle q^2 \right\rangle \left\langle \Delta r^2 \right\rangle \approx 1$$

which gives $\sqrt{\left\langle \Delta r^2 \right\rangle} \approx \frac{\lambda l^*}{9L}$. This shows that the length scale that the particle motion can be probed by transmission DWS is much smaller than λ while in weak scattering regime, the length scales probed are greater or equal to wavelength. The effect of hydrodynamic interactions for time scales corresponding to particle motion at the angstrom level have been reported [59]. Using DWS for heavily scattering medium, the time scales can be controlled by varying the sample thickness. The thickness is often chosen to be in the range $5 < L/l^* < 20$. Typically, the diffusion approximation used in DWS is not acceptable for thicknesses smaller than 5 [41].

1.2.c Backscattering:

For studying backscattering, the light is uniformly incident on a face of an otherwise infinite slab of thickness, L [28-30,32]. The source is a delta function pulse deposited at zpl^*. In backscattering, the light is detected from the illuminated face. The detected intensity of the pulse source is shown in figure 4. The intensity peaks sharply and then

decays slowly. The peak occurring at very early times shows that most of the photons are back scattered without migrating deep into the sample. A few scattering events are enough to scatter them back. The subsequent decay of the backscattering function is due to the contributions from paths of greater lengths. Consequently, as seen in figure 4, there is a much broader distribution of time scales in the decay as compared to figure 3.

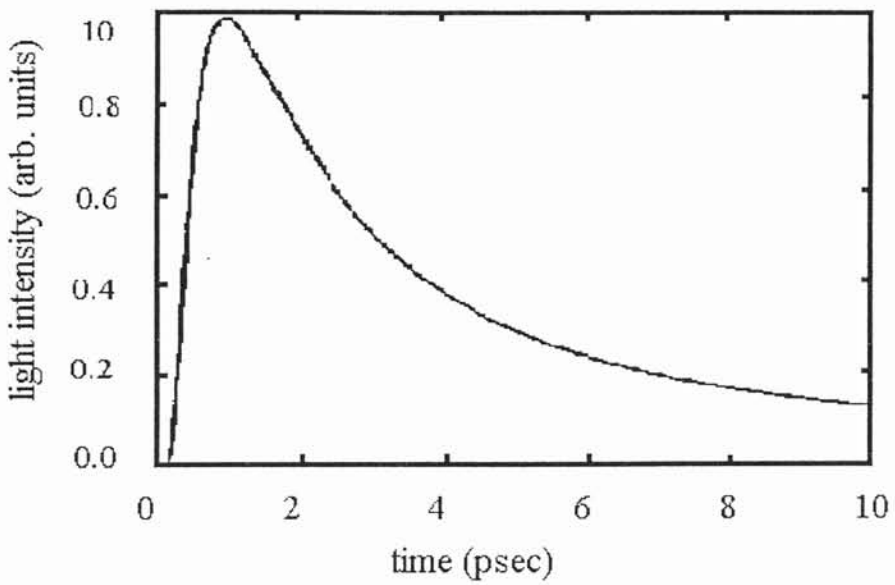

Fig.4- The dependence of the detected backscattered intensity of an incident delta function pulse sent on a sample with $L = 1mm$ and $l^* = 100\mu m$.

The information about the decay in intensity is again embodied in $P(s)$. However, extending the limits of integration in Eq.1.2.14 from $s = 0$ to $s = \infty$ does not lead to sensible result for backscattering geometry. At least one scattering event is needed for us to talk about backscattering. This fact requires $n \geq 1$. Therefore, the lower bound of integration should be taken at least l_s. To ensure this, the source of diffusing intensity

has been taken at a distance of zpl^* with $zp \geq 1$ inside the illuminated face. For the backscattering geometry, the unnormalized correlation function is calculated to be

$$G_B(x) = \frac{Sinh[\sqrt{x}(\widetilde{L} - zp] + z_e\sqrt{x}Cosh[\sqrt{x}(\widetilde{L} - zp)]}{(1 + z_e{}^2 x)Sinh\widetilde{L}\sqrt{x} + 2z_e\sqrt{x}Cosh\widetilde{L}\sqrt{x}} \tag{1.2.21}$$

For a sample of infinite thickness, $L \to \infty$, all light is backscattered and Eq.1.2.21 becomes

$$G_B(x) = g_B(x) = \frac{e^{-zp\sqrt{x}}}{1 + z_e\sqrt{x}} \tag{1.2.22}$$

Several authors identify zp with the average value $\langle zp \rangle$ of the position of the source [8,32,42]. The experiments show that the decay of the correlation function is exponential in the square root of time. This suggests

$$G_B(x) = g_B(x) = e^{-\gamma\sqrt{x}} \cong 1 - \gamma\sqrt{x} + \ldots \tag{1.2.23}$$

where $\gamma = \langle zp \rangle + z_e$ to be consistent with a small time expansion of Eq.1.2.22. When $|g_B(x)|^2$ is plotted logarithmically as a function of $\sqrt{x}$, a linear graph, where the slope is γ results. However, circularly polarized light differs in γ from linearly polarized light. It has been shown that the dependence of γ on polarization is strongest for isotropic scatterers and becomes weaker as l^*/l_s ratio becomes larger [11]. Detailed explanation on the behavior of γ will be given later in the thesis.

In summary, DWS extends the application of QELS to multiple-scattering regimes. However, it has its limits of application. It fails to fully describe the transport of light for thin slabs [41]. Several methods have been used, one of which, based on the

radiation transfer equation, was proposed by Ackerson, Dougherty and co-workers [43,44] to improve DWS. MacKintosh and John developed a filed theory method that describes the nondiffusive propagation of light at distances smaller than transport mean free path [45]. Within the diffusion approximation the correct treatment of scattering anisotropy, multiple reflections are not also allowed. Of particular interest is the two-stream theory proposed by Durian that solves the propagation of light through optically dense media analytically without invoking diffusion approximation [47].

1.3 Two-Stream Theory

1.3.1 Time-dependent two-stream equations

Durian proposed two-stream theory that studies the transmitted and the backscattered light, from an optically dense random medium without using diffusion approximation. The two-stream theory approximates the scattering photons by two counter propagating concentration fields, $I_d(z,t)$ and $I_u(z,t)$. We take the two directions to be up (u) and down (d), upon scattering. Since this treatment is only in one dimension, z, the scattering angle is not a continuum variable and the model becomes soluble.

The time dependent two-stream equations are constructed by considering the mechanisms that change the number of photons in a given direction. The photons are added to or lost from a beam upon scattering. For example, absorption produces a loss in the total number of photons. Taking all possible mechanisms into account the change in the intensity can be written:

$$I_d(z,t+\Delta t) - I_d(z,t) = [I_d(z,t) + (c\Delta t / l_s)(1-p) I_u(z+c\Delta t,t)] - [(c\Delta t / l_a) I_d(z,t) + (c\Delta t / l_s)(1-p) I_d(z,t) + I_d(z+c\Delta t,t)] \quad (1.3.1.a)$$

$$I_u(z+c\Delta t,t+\Delta t)-I_u(z+c\Delta t,t)=[I_u(z+c\Delta t,t)+(c\Delta t/l_s)(1-p)I_d(z,t)]-[(c\Delta t/l_a)I_u(z+c\Delta t,t)$$
$$+(c\Delta t/l_s)(1-p)I_u(z+c\Delta t,t)+I_u(z,t)] \qquad (1.3.1.b)$$

These equations give the change of the downward and upward going stream intensities in a length element, $[z, z+c\Delta t]$, during a time interval Δt, respectively. Here, l_a stands for the absorption length and p for the fraction of photons, which go into the forward direction upon scattering. The terms in the first set of brackets on the rhs represent the intensity that flows in, and that is transferred from the other stream. The terms in the second set of brackets are the number of photons that are absorbed from, that scatter out and that flow out, respectively.

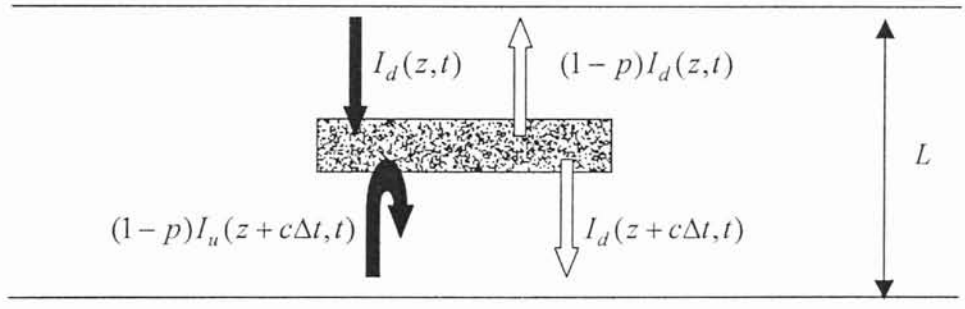

Fig.5- Schematic representation showing the gains (filled arrows) and losses (empty arrows) of downward intensity.

Figure 5 shows the mechanisms that change the number of photons in the downward intensity. The filled straight arrow represents the intensity that flows in, the filled curved arrow represents the intensity that scatter in, the downward empty arrow represents the intensity that flows out and the upward empty arrow represents the intensity that scatter out.

The average cosine of the two possible scattering angles may be expressed in terms of p as $<\mu>= 1(p)+(-1)(1-p) = 2p-1$ which leads to $l_s / l^* = 1-\langle\mu\rangle = 2(1-p)$. Taking the limit $\Delta t \to 0$ and neglecting absorption the following differential equations result:

$$-\frac{\partial I_d}{\partial t} = \frac{\partial I_d}{\partial z} + \frac{1}{2z_0}(I_d - I_u) \tag{1.3.2.a}$$

$$\frac{\partial I_u}{\partial t} = \frac{\partial I_u}{\partial z} + \frac{1}{2z_0}(I_d - I_u) \tag{1.3.2.b}$$

These equations are expressed in reduced units, where $z \to z/l^*$ and $t \to tc/l^*$. For applications to three-dimensions [48] and to extend the utility of the equations to thick samples and isotropic scattering, a dimensionality parameter, z_0, is added. For a truly one-dimensional problem its value is 1. The results of these equations are also valid for very short length scales for which the light propagation is ballistic. The transmitted and backscattered fluxes can be deduced from Eqs.1.3.2 by using the appropriate boundary conditions.

1.3.2 Results for DTS

Diffuse Transmission Spectroscopy is a technique where the probability, T_p, that an incident photon will be diffusely transmitted through an opaque sample is measured. The transmission probability is given in terms of the ratio of the sample thickness to the transport mean free path [49]. Eq.1.2.18 is the DTS prediction for the transmitted photons. The prediction of two-stream theory for the transmission probability is achieved by time-independent solutions of Eqs.1.3.2 with the following boundary conditions:

$$I_d(0) = RI_u(0) \quad , \quad I_u(\tilde{L}) = RI_d(\tilde{L}) \tag{1.3.3}$$

where R is the boundary reflectivity. Eqs.1.3.4 presents solutions for $z < zp$ and $z > zp$.

$$I_d(z) + I_u(z) = \frac{I_0}{z_0}\begin{cases}\left(z + z_0\dfrac{1+R}{1-R}\right)(1-T_p) & z < zp \\ \left(\tilde{L} - z + z_0\dfrac{1+R}{1-R}\right)T_p & z > zp\end{cases} \tag{1.3.4.a}$$

$$I_d(z) - I_u(z) = I_0\begin{cases}1-T_p & z < zp \\ T_p & z > zp\end{cases} \tag{1.3.4.b}$$

Here, I_0 is the intensity of the incident light. These solutions also agree with the expected conditions $(1-R)I_d(\tilde{L}) = I_0T_p$ and $(1-R)I_u(0) = I_0(1-T_p)$. The plus solution Eq.1.3.4.a indicates that the photon concentration extrapolates to zero at $z_0(1+R)/(1-R)$ outside the edges of the sample. This is consistent with the extrapolation depth ratio introduced in DWS theory. The minus solution, Eq.1.3.4.b being nonzero, indicates that the photon velocities are not directed isotropically which is contrary to DWS. According to two-stream theory, this happens only for $z < zp$ when the sample is thick or across the entire sample for thinner slabs. This difference is due to the discontinuity of the streams at originating zp due to the scattering probability p of the deposited light and can be specified as:

$$\frac{I_d(zp^+) - I_d(zp^-)}{I_u(zp^-) - I_u(zp^+)} = \frac{p}{1-p} \tag{1.3.5}$$

Eq.1.3.5 with Eqs.1.3.4 gives the two-stream result for the diffuse transmission probability:

$$T_p = \frac{zp + z_0(2p-1) + z_0(1+R)/(1-R)}{\widetilde{L} + 2z_0(1+R)/(1-R)} \tag{1.3.6}$$

For the case of isotropic scattering, where $p = 1/2$, Eq.1.3.6 reduces to Eq.1.2.18 with $z_e = z_0(1+R)/(1-R)$. Taking the integral over a range of penetration depths, we obtain a general transition probability result. Multiple reflections at the boundaries, which we ignored in DWS, can also be taken into consideration. To do this, the probability for an incident photon to cross the sample without scattering and then reflect, $F = R_b e^{-L/l_s}$, is considered in the calculation. Here, R_b, is the ballistic reflection probability.

$$T_{p'} = \frac{1}{1-F^2}\int_0^{\widetilde{L}} [T_p + F(1-T_p)]e^{-zpl^*/l_s} l^*/l_s dzp$$

$$= \frac{\left[\frac{l_s}{l^*} + z_0(2p-1) + z_0\left(\frac{1+R}{1-R}\right)\left(\frac{1+F}{1-F}\right)\right](1-e^{-L/l_s})}{\left[\widetilde{L} + 2z_0\left(\frac{1+R}{1-R}\right)\right](1+F)} - \frac{\widetilde{L}(1-R_b)e^{-L/l_s}}{\left[\widetilde{L} + 2z_0\left(\frac{1+R}{1-R}\right)\right](1-F^2)} \tag{1.3.7}$$

This result applies for arbitrary slab thickness, boundary reflectivity and scattering anisotropy. An exact result is obtained for one-dimensional problems with $z_0 = 1$. Durian has also showed that with the choice of $z_0 = 2/3$ [38] a better result for three-dimensional case is achieved compared to the DWS predictions [47]. In the limit of strong scattering, where the scattering is isotropic, Eq.1.3.7 reduces to Eq.1.2.18. When the limit of anisotropic scattering is considered, where $p \to 1$, Eq.1.3.7 gives

$$T_p = \frac{2z_0/(1-R)}{\widetilde{L} + 2z_0(1+R)/(1-R)} \tag{1.3.8}$$

The accuracy of Eq.1.3.7 is also tested with random walk computer simulations [38,50].

1.3.3 Results for DWS

The predictions of two-stream theory for DWS are achieved by taking the Laplace transform of the time-dependent Eqs.1.3.2. While doing this, the light source is considered a down going instantaneous source at a distance zp from the edge of the sample. Thus, the light source can be taken as a delta function in position and expressed at the initial deposition time as

$$I_d(z,0) = p\delta(z - zp) \tag{1.3.9.a}$$

$$I_u(z,0) = (1-p)\delta(z - zp) \tag{1.3.9.b}$$

1.3.3.a Results for Transmission

For transmission geometry, we start with differential equations given in Eqs.1.3.2. Taking the Laplace transform and implementing the source boundary conditions given in Eqs.1.3.9, the Laplace transform of the downward and upward intensities are found to be

$$\bar{I}_d(z,\omega) = \left(\frac{1}{4z_0\alpha} + \frac{p\omega}{2\alpha} \pm \frac{p}{2}\right)e^{-\alpha|z-zp|} + A_1 e^{\alpha z} + A_2 e^{-\alpha z} \tag{1.3.10.a}$$

$$\bar{I}_u(z,\omega) = \left(\frac{1}{4z_0\alpha} + \frac{(1-p)\omega}{2\alpha} \mp \frac{1-p}{2}\right)e^{-\alpha|z-zp|} + A_1(1+2z_0(\omega+\alpha))e^{\alpha z} + A_2(1+2z_0(\omega-\alpha))e^{-\alpha z} \tag{1.3.10.b}$$

which yield different results for $z > zp$ and $z < zp$. Here, $\alpha = \sqrt{\omega(\omega + 1/z_0)}$ where ω is the transformed time variable and the constants A_1 and A_2 are determined by the following bou.ndary conditions

$$\bar{I}_d(0,\omega) = R\bar{I}_u(0,\omega) \tag{1.3.11.a}$$

$$\bar{I}_u(\tilde{L},\omega) = R\bar{I}_d(\tilde{L},\omega) \tag{1.3.11.b}$$

Now, applying these two boundary conditions to Eq.13.10.a and solving for the transmitted pulse gives

$$(1-R)\bar{I}_d(\tilde{L},\omega) = \frac{\left[1+2z_0\left(\frac{p-R(1-p)}{1-R}\right)\omega\right]Sinh(\alpha\, zp) + 2z_0\left(\frac{p+R(1-p)}{1-R}\right)\alpha\, Cosh(\alpha\, zp)}{\left(1+2z_0\frac{(1+R^2)}{(1-R)^2}\omega\right)Sinh(\alpha\tilde{L}) + 2z_0\left(\frac{1+R}{1-R}\right)\alpha\, Cosh(\alpha\tilde{L})} \tag{1.3.12}$$

Taking a Laplace inverse of this result will give the time-dependent emission for a pulse $P(s)$. Recall that Eq.1.2.14 relates the Laplace transform of $P(s)$ to $G(\tau)$. Thus Eq.1.3.12 is the unnormalized field correlation function ,

$$G_T(x) = \frac{\left[1+2z_0{}^2\left(\frac{p-R(1-p)}{1-R}\right)x\right]Sinh(\alpha\, zp) + 2z_0\left(\frac{p+R(1-p)}{1-R}\right)\alpha\, Cosh(\alpha\, zp)}{\left(1+2z_0{}^2\frac{(1+R^2)}{(1-R)^2}x\right)Sinh(\alpha\tilde{L}) + 2z_0\left(\frac{1+R}{1-R}\right)\alpha\, Cosh(\alpha\tilde{L})}, \tag{1.3.13}$$

where $x = \omega / z_0$ gives $\alpha = \sqrt{x(1+z_0{}^2 x)}$. To obtain the normalized form, Eq.1.3.13 should be divided by diffuse transmission probability, T_p given by $T_p = (1-R)\bar{I}_d(\tilde{L},0)$. Taking the average over penetration depths as in Eq.1.2.19, the normalized transmission autocorrelation function for arbitrary thickness with no multiple reflections is found as in Eq.1.3.14,

$$g_T(x)=\frac{\left(A+B\frac{l^*}{l_s}\right)\alpha-\left[\left(A\frac{l^*}{l_s}+B\alpha^2\right)Sinh(\tilde{L}\alpha)+\left(A+B\frac{l^*}{l_s}\right)\alpha Cosh(\tilde{L}\alpha)\right]e^{-L/l_s}}{T_p{}'\frac{l_s}{l^*}\left[\left(\frac{l^*}{l_s}\right)^2-\alpha^2\right]\left[\left(1+2z_0{}^2\frac{(1+R^2)}{(1-R)^2}x\right)Sinh(\alpha\tilde{L})+2z_0\left(\frac{1+R}{1-R}\right)\alpha Cosh(\alpha\tilde{L})\right]}$$

(1.3.14)

where $A=1+2z_0{}^2x(p-R(1-p))/(1-R)$ and $B=2z_0(p+R(1-p))/(1-R)$. This equation represents an improvement to DWS result in Eq.1.2.20.

1.3.3.b Results for backscattering

Applying the same boundary conditions, Eq.1.3.11 but this time solving for Eq.1.3.10.b, the backscattered pulse is computed as

$$(1-R)\bar{I}_u(0,\omega)=\frac{\left[1+2z_0\left(\frac{1-p(1+R)}{1-R}\right)\omega\right]Sinh\alpha(\tilde{L}-zp)+2z_0\left(\frac{1-p(1-R)}{1-R}\right)\alpha Cosh\alpha(\tilde{L}-zp)}{\left(1+2z_0\frac{(1+R^2)}{(1-R)^2}\omega\right)Sinh(\alpha\tilde{L})+2z_0\left(\frac{1+R}{1-R}\right)\alpha Cosh(\alpha\tilde{L})}$$

(1.3.15)

To generate the two-stream prediction for backscattering autocorrelation function, we simply evaluate Eq.1.3.15 at $\omega=xz_0$, as done in the case of transmission, that yields

$$G_B(x)=\frac{\left[1+2z_0{}^2\left(\frac{1-p(1+R)}{1-R}\right)x\right]Sinh\alpha(\tilde{L}-zp)+2z_0\left(\frac{1-p(1-R)}{1-R}\right)\alpha Cosh\alpha(\tilde{L}-zp)}{\left(1+2z_0{}^2\frac{(1+R^2)}{(1-R)^2}x\right)Sinh(\alpha\tilde{L})+2z_0\left(\frac{1+R}{1-R}\right)\alpha Cosh(\alpha\tilde{L})}.$$

(1.3.16)

This result is more accurate than DWS prediction, Eq.1.2.21. The reason lies in the fact that distances smaller than the transport mean free path has an important role in backscattering and they cannot be described correctly within diffusion approximation. The normalized correlation function is reached by dividing Eq.1.3.16 by the diffuse backscattering probability, $1-T_p$, that obeys $1-T_p=(1-R)\bar{I}_u(0,0)$. The final result for a semi-infinite slab, for which T_p goes to zero, after averaging over penetration depths, is presented in Eq.1.3.17.

$$g_B(x)=\frac{1+2z_0{}^2\left(\frac{1-p(1+R)}{1-R}\right)x+2z_0\left(\frac{1-p(1-R)}{1-R}\right)\alpha}{1+2z_0{}^2\frac{(1+R^2)}{(1-R)^2}x+2z_0\left(\frac{1+R}{1-R}\right)\alpha}\left[\frac{l^*/l_s}{(l^*/l_s)+\alpha}\right] \qquad (1.3.17)$$

The improvement achieved by two-stream theory over diffusion theory has also been demonstrated by comparison with the random walk simulation results [47]. The main advantage of two-stream approach is that, the results apply for arbitrary slab thickness, scattering anisotropy and boundary reflectivity. This increases the accuracy of diffusing light spectroscopies and extends their range of validity to thinner, more experimentally accessible samples. Furthermore, time dependent two-stream equations 1.3.2.a and 1.3.2.b characterize not only the diffusive motion of photons for long paths but also ballistic motion for short length scales.

1.4 This Thesis

Polarization becomes a consideration when working with the scattering of light. Since the light is polarized, both the polarization of light and the direction of propagation change, upon scattering. In recent years, there has been an increasing interest in the propagation of polarized light in randomly scattering media since it is used in all aspects of optical technology. Significant progress has been made in remote sensing for underwater [51], atmospheric [52] and biological [53,54] imaging. Polarized light is also used in geophysical engineering as well as industrial metrology. The investigation of backscattered polarized light is of particular interest in medical applications [23-26]. The widely used technique in analyzing the propagation of light through an optically dense random medium is DWS. However, the effects of multiple scattering on a polarized beam are not obvious and difficult to consider in diffusive wave spectroscopy. In this thesis, a theoretical model to explain the underlying reason for the observed polarization dependence behavior of light transmitted or backscattered from an optically dense medium will be developed based on two-stream theory. In our model, the scattered photons will be studied in four streams instead of two. We will follow the same steps as in two-stream to reach our dynamic four-stream results. But, before starting the derivation of four-stream equations, we consider the transition probabilities and their microscopic definitions.

Chapter 2

Transition Probabilities in a Four-Stream Theory

We now generalize the Durian two-stream theory to include polarization. The treatment in one dimension, introduced in two-stream theory is still assumed: The scattered photons are represented by two beams, upward (u) and downward (d). However, in addition, two orthogonal polarization states are assigned to each direction, giving a total of four beams: $I_{dp}, I_{dm}, I_{up}, I_{um}$. The first index indicates the propagation direction ("up" or "down") while the second indicates the type of polarization ("positively polarized" or "negatively polarized"). The two mutually orthogonal polarization states can be horizontal and vertical in the case of linear polarization or right and left circular in the case of circular polarization. The phase difference between scattered waves and the phase relation between two orthogonal polarization states of a single photon are ignored within the theory.

2.1 Introduction of Transition Probabilities

In Durian's two-stream model, there are two possible transition probabilities: p is the fraction of photons, which go into the forward direction and $1-p$ is the fraction that change direction. In the four-stream theory, the scattered photons can either change direction, polarization, or both. There are now 16 possible transition probabilities.

p_{udpm}	p_{udmp}	p_{dupm}	p_{dump}
p_{udpp}	p_{udmm}	p_{dupp}	p_{dumm}
p_{uupm}	p_{uump}	p_{ddpm}	p_{ddmp}
p_{uupp}	p_{uumm}	p_{ddpp}	p_{ddmm}

Table-1: Possible transition probabilities in four-stream model.

Here, p_{dupm} is the transition probability that a photon directed downward with positive polarization is scattered upward with negative polarization. Similar definitions hold for the other probabilities. Because the scattering medium is assumed isotropic, all elements in the same row of table-1 must be equal. The fact that the number of photons is conserved in the scattering processes requires the summation of each column to be one. Furthermore, Durian's p consists of two terms. For example, for downward positive intensity p is expressed as $p_{ddpp} + p_{ddpm}$ which is independent of polarization.

2.2 Introduction of Microscopic Parameters

Before constructing and solving the four-stream model, we need to connect the transition probabilities to single particle scattering characteristics that can be measured independently or modeled theoretically. One of the microscopic parameters is the asymmetry parameter, g, that corresponds to the average cosine of the scattering angle introduced as $<\mu>=1(p)+(-1)(1-p)$ in two-stream model. In four-flux theory, g has the same meaning as before. It is the mean cosine of the scattered intensity independent of the state of polarization. Basically, it specifies the degree of anisotropy of the

scattering process. For example, for the downward positively polarized intensity, its value becomes $g_{(dp)} = (p_{ddpp} + p_{ddpm}) + (-1)(p_{dupp} + p_{dupm})$. Two other microscopic parameters that will be used in calculations are σ and $g_c : \sigma$ refers to the probability that polarization state remains unchanged by scattering and g_c refers to polarization difference asymmetry. For I_{dp}, σ is $\sigma_{(dp)} = p_{ddpp} + p_{dupp}$ and g_c is $g_{c(dp)} = (p_{ddpp} - p_{ddpm}) + (-1)(p_{dupp} - p_{dupm})$. Other intensities, I_{dm}, I_{up}, I_{um} have numerically the same σ and g_c values due to the isotropy properties of the p given in table-1.

The asymmetry parameters g has been defined in terms of single particle scattering intensities and evaluated using Mie theory with great success [55]. Therefore, we adopt this method to define the microscopic parameters σ, g and g_c. The definitions of these parameters are given below, I_p, I_m indicating the single particle scattered intensities with positive and negative polarizations, respectively, given an incident positive polarization. Note that the integration is over a continuous distribution of scattering angles, not just forward and backward directions.

$$\sigma = \frac{\int I_p(\mu) d\mu}{\int (I_p(\mu) + I_m(\mu)) d\mu} \tag{2.2.1.a}$$

$$g = \frac{\int (I_p(\mu) + I_m(\mu)) \mu d\mu}{\int (I_p(\mu) + I_m(\mu)) d\mu} \tag{2.2.1.b}$$

$$g_c = \frac{\int (I_p(\mu) - I_m(\mu)) \mu d\mu}{\int (I_p(\mu) + I_m(\mu)) d\mu} \tag{2.2.1.c}$$

The normalization is achieved by dividing by the total scattered intensity integrated over all angles. It is clear that σ is the probability that a given state of polarization survives scattering, g is the mean cosine of the total intensity averaged over all scattering angles and g_c is the mean cosine of the polarization difference intensities averaged over all scattering angles upon a single scattering.

Polarization states may be defined by Stokes Theory of polarization and used to obtain the numerical estimates of microscopic parameters. Upon scattering from spherically symmetric, optically inactive particles the scattered wave, which is generally elliptically polarized, is expressed using Stokes Matrix formalism. For example, for a right-circularly polarized beam incident on the particle, the scattered intensity at an angle θ becomes

$$I_s(\theta) = \begin{bmatrix} S_{11}(\theta) & S_{12}(\theta) & 0 & 0 \\ S_{12}(\theta) & S_{11}(\theta) & 0 & 0 \\ 0 & 0 & S_{33}(\theta) & S_{34}(\theta) \\ 0 & 0 & -S_{34}(\theta) & S_{33}(\theta) \end{bmatrix} \begin{bmatrix} 1 \\ 0 \\ 0 \\ 1 \end{bmatrix} I_0 = \begin{bmatrix} S_{11}(\theta) \\ S_{12}(\theta) \\ S_{34}(\theta) \\ S_{33}(\theta) \end{bmatrix} I_0 \tag{2.2.2}$$

where the 4×4 matrix is an amplitude-scattering matrix and the column matrix times I_0 stands for the incident right-circularly polarized beam. The elements of the amplitude scattering matrix are

$$\begin{aligned} S_{11}(\theta) &= 1/2\left(|S_2|^2 + |S_1|^2\right) \\ S_{12}(\theta) &= 1/2\left(|S_2|^2 - |S_1|^2\right) \\ S_{33}(\theta) &= 1/2\left(S_1 S_2^* + S_2 S_1^*\right) \\ S_{34}(\theta) &= i/2\left(S_1 S_2^* - S_2 S_1^*\right) \end{aligned} \tag{2.2.3}$$

where S_1 and S_2 are scattering parameters that relate the incident and scattered electric field components using Mie scattering theory [51]. For an incoming circularly polarized

light to the detector, the resultant detected intensity for right or left circularly polarized light is determined using the appropriate matrix forms for right and left circular analyzers.

$$I_R = \frac{1}{2}\begin{bmatrix} 1 & 0 & 0 & 1 \\ 0 & 0 & 0 & 0 \\ 0 & 0 & 0 & 0 \\ 1 & 0 & 0 & 1 \end{bmatrix} I_S = \frac{1}{2}\begin{bmatrix} S_{11}(\theta) + S_{33}(\theta) \\ 0 \\ 0 \\ S_{11}(\theta) + S_{33}(\theta) \end{bmatrix} I_0 \qquad (2.2.4.a)$$

$$I_L = \frac{1}{2}\begin{bmatrix} 1 & 0 & 0 & -1 \\ 0 & 0 & 0 & 0 \\ 0 & 0 & 0 & 0 \\ -1 & 0 & 0 & 1 \end{bmatrix} I_S = \frac{1}{2}\begin{bmatrix} S_{11}(\theta) - S_{33}(\theta) \\ 0 \\ 0 \\ S_{11}(\theta) - S_{33}(\theta) \end{bmatrix} I \qquad (2.2.4.b)$$

The difference between the first elements of the Stokes vectors I_R and I_L gives the degree of circular polarization and the sum gives the total scattered intensity. Thus $I_{degree} = S_{33}(\theta)$ and $I_{total} = S_{11}(\theta)$ such that σ and g factors are written as

$$\sigma = \frac{1/2\int(S_{11} + S_{33})d\mu}{\int S_{11}d\mu} \qquad (2.2.5.a)$$

$$g = \frac{\int S_{11}\mu d\mu}{\int S_{11}d\mu} \qquad (2.2.5.b)$$

$$g_c = \frac{\int S_{33}\mu d\mu}{\int S_{11}d\mu} \qquad (2.2.5.c)$$

The microscopic definitions of α and g_c for linearly polarized light are more ambiguously defined.

$$\alpha = \frac{\int\left[3/8(S_{11} - S_{12})\mu^2 + 1/4S_{33}\mu + 3/8(S_{11} + S_{12})\right]d\mu}{\int S_{11}d\mu} \qquad (2.6.a)$$

$$g_c = \frac{\int\left[3/4(S_{11}-S_{12})\mu^2 + 1/2S_{33}\mu + 3/4(S_{11}+S_{12}) - S_{11}\right]\mu d\mu}{\int S_{11} d\mu} \qquad (2.6.b)$$

As the degree of projection of the final polarization direction along the incident direction. Figures 6 and 7 show the σ and g factors evaluated by Ackerson and Tata [55] for circular and linear polarization states for a range of $ka = 2\pi a/\lambda$, a being the particle radius and λ the radiation wavelength in vacuum. The particle and suspending refractive indexes are 1.59 and 1.33, respectively. Linear and circular polarizations evidence quite different properties on single scattering. For wavelengths large compared to particle radius, linear polarization tends to be scattered isotropically $(g_c \to 0)$ but the state of polarization is preserved $(\sigma \to 0.8)$. For circular polarization there is a spin flip on backscattering compared to forward scattering $(g_c \to 0.5)$ and single scattering randomizes the polarization $(\sigma \to 0.5)$. In the opposite limit all particles tend to scatter more in the forward direction $(g, g_c \to 1)$ and the state of polarization is preserved $(\sigma \to 1)$, though much more completely for circular polarization.

Because of the conditions imposed on the transition probabilities in table-1, there are only three independent parameters needed to define all 16 values. These parameters are taken as those given in Eqs.2.2.5 to find,

$$p_{udpm} = (2 - g - 2\sigma + g_c)/4 \qquad (2.2.5.a)$$

$$p_{udpp} = (-g + 2\sigma - g_c)/4 \qquad (2.2.6.b)$$

$$p_{uupm} = (2 + g - 2\sigma - g_c)/4 \qquad (2.2.6.c)$$

$$p_{uupp} = (g + 2\sigma + g_c)/4 \qquad (2.2.6.d)$$

and so on.

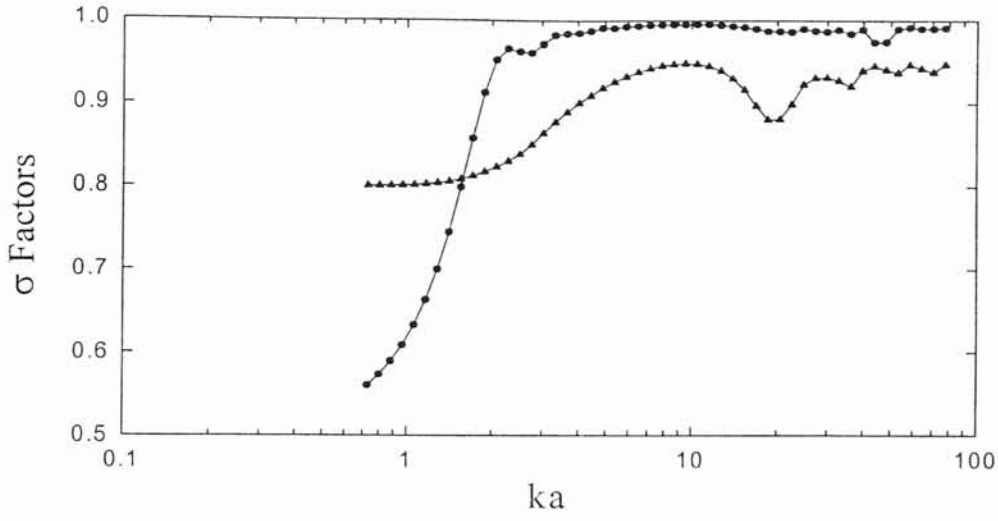

Fig.6- The σ factors for circular (solid circles) and linear (solid triangles) polarization as a function of ka for spherical particles with index of refraction 1.59 in a solvent with index of refraction 1.33. (Polystyrene spheres in water)

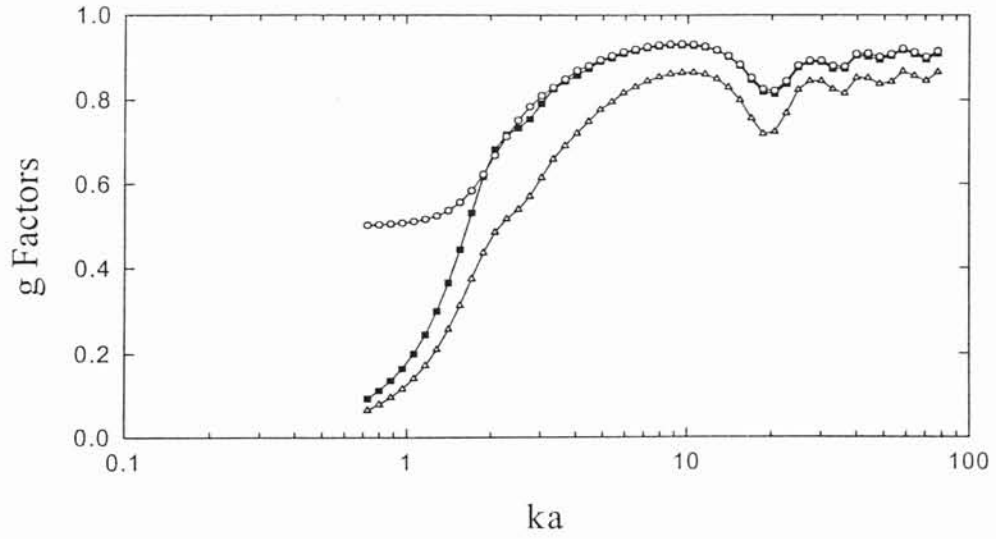

Fig.7- Scalar asymmetry parameter, g (solid squares), and polarization difference asymmetry factors, g_c, for circular (circles) and linear (triangles) polarization as a function of ka for spherical particles with index of refraction 1.59 in a solvent with index of refraction 1.33. (Polystyrene spheres in water)

Chapter 3

Dynamic Four-Stream Model for Polarization

3.1 Time-dependent Four-Flux Equations

We are ready to develop dynamic solutions for the total transmitted and the backscattered intensities as well as the transmitted and the backscattered intensities that show the degree of polarization, using a four-stream model. The same steps leading to Durian's two-stream theory will be followed. However, here, a matrix formulation proves useful. Let us begin with writing four-types of intensities $I_{dp}, I_{dm}, I_{up}, I_{um}$ in a matrix form:

$$I = \begin{pmatrix} I_{dp} \\ I_{dm} \\ I_{up} \\ I_{um} \end{pmatrix} \tag{3.1.3}$$

The first indices indicate the propagation direction ("up" or "down"), while the second indices give the type of polarization, "plus" or "minus". As in two-stream theory, we start with the development of the time-dependent equations. To do that, all possible mechanisms that change the intensity, in a given direction and a given polarization, in a length element $[z, z + c\Delta t]$ during a time interval Δt are considered. Since the polarization is included, the polarization difference asymmetry, g_c, and the probability of unchanged polarization state, σ will ultimately appear in the equations along with the asymmetry parameter, g.

$$I_{dp}(z,t+\Delta t)-I_{dp}(z,t)=I_{dp}(z,t)+\frac{c\Delta t}{\ell_s}\left(p_{udpp}I_{up}(z+c\Delta t,t)+p_{udmp}I_{um}(z+c\Delta t,t)+p_{ddmp}I_{dm}(z,t)\right)$$
$$-\left(\frac{c\Delta t}{\ell_a}I_{dp}(z,t)+\frac{c\Delta t}{\ell_s}(p_{dupp}+p_{dupm}+p_{ddpm})I_{dp}(z,t)+I_{dp}(z+c\Delta t,t)\right)$$

(3.1.2.a)

$$I_{dm}(z,t+\Delta t)-I_{dm}(z,t)=I_{dm}(z,t)+\frac{c\Delta t}{\ell_s}\left(p_{udmm}I_{um}(z+c\Delta t,t)+p_{udpm}I_{up}(z+c\Delta t,t)+p_{ddpm}I_{dp}(z,t)\right)$$
$$-\left(\frac{c\Delta t}{\ell_a}I_{dm}(z,t)+\frac{c\Delta t}{\ell_s}(p_{dumm}+p_{dump}+p_{ddmp})I_{dm}(z,t)+I_{dm}(z+c\Delta t,t)\right)$$

(3.1.2.b)

$$I_{up}(z+c\Delta t,t+\Delta t)-I_{up}(z+c\Delta t,t)=I_{up}(z+c\Delta t,t)+\frac{c\Delta t}{\ell_s}\left(p_{dupp}I_{dp}(z,t)+p_{dump}I_{dm}(z,t)+p_{uump}I_{um}(z+c\Delta t,t)\right)$$
$$-\left(\frac{c\Delta t}{\ell_a}I_{up}(z+c\Delta t,t)+\frac{c\Delta t}{\ell_s}(p_{udpp}+p_{udpm}+p_{uupm})I_{up}(z+c\Delta t,t)+I_{up}(z,t)\right)$$

(3.1.2.c)

$$I_{um}(z+c\Delta t,t+\Delta t)-I_{um}(z+c\Delta t,t)=I_{um}(z+c\Delta t,t)+\frac{c\Delta t}{\ell_s}\left(p_{dumm}I_{dm}(z,t)+p_{dupm}I_{dp}(z,t)+p_{uupm}I_{up}(z+c\Delta t,t)\right)$$
$$-\left(\frac{c\Delta t}{\ell_a}I_{um}(z+c\Delta t,t)+\frac{c\Delta t}{\ell_s}(p_{udmm}+p_{udmp}+p_{uump})I_{um}(z+c\Delta t,t)+I_{um}(z,t)\right)$$

(3.1.2.d)

These equations give the change in intensities, $I_{dp}, I_{dm}, I_{up}, I_{um}$, respectively. The first term on the right-hand side of each equation represents the intensity that flows in, the terms in the first set of brackets represent the intensities that scatter in, the last three terms in the second set of brackets represent the intensities that are absorbed from, that are scattered out of and that flow out, respectively. Figure 8 shows the mechanisms that change the number of photons in the downward positive intensity.

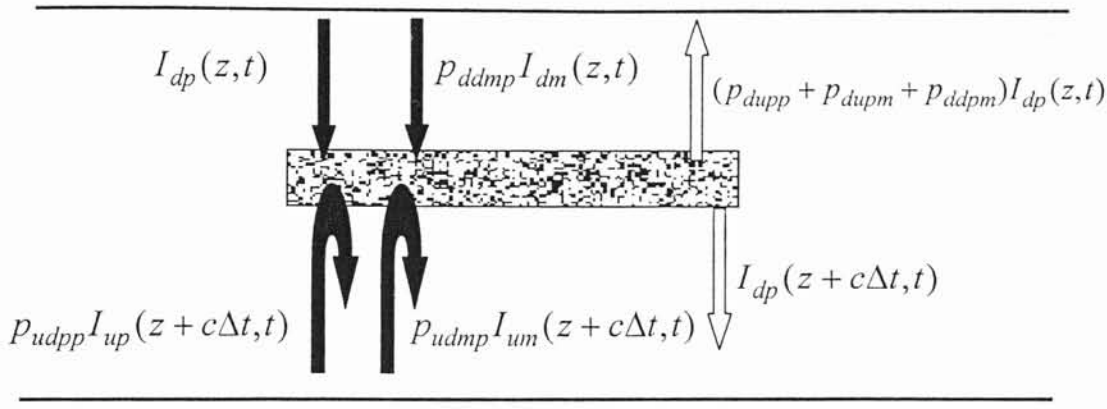

Fig.8- Schematic representation showing the gains (filled arrows) and losses (empty arrows) of downward positive intensity.

Taking the limit $\Delta t \to 0$, making the change of variables $t \to ct/\ell_s$ and $z \to z/\ell_s$ and multiplying both sides by ℓ_s/c the following differential matrix equation results:

$$\frac{d}{dt}[I] = \frac{d}{dz}[N][I] + [M][I] \tag{3.1.3}$$

where

$$[\mathrm{M}] = \frac{1}{z_0}\begin{pmatrix} -(p_{dupp}+p_{dupm}+p_{ddpm})-\kappa & p_{ddmp} & p_{udpp} & p_{udmp} \\ p_{ddpm} & -(p_{dumm}+p_{dump}-p_{ddmp})-\kappa & p_{udpm} & p_{udmm} \\ -p_{dupp} & -p_{dump} & p_{udpp}+p_{udmp}+p_{uupm}+\kappa & -p_{uump} \\ -p_{dupm} & -p_{dumm} & -p_{uupm} & p_{udmm}+p_{udmp}+p_{uump}+\kappa \end{pmatrix} \tag{3.1.4}$$

and

$$[N] = \begin{pmatrix} -1 & & & \\ & -1 & & \\ & & 1 & \\ & & & 1 \end{pmatrix} \tag{3.1.5}$$

with $\kappa = l_s / l_a$ defining the dimensionless absorption factor. The sign changes in the third and forth row of matrix $[M]$ because the downward intensity is attenuated in the direction of increasing z whereas the upward intensity is attenuated in the direction of decreasing z, as in two-stream theory.

For applications to three dimensions, z_0 is added in all four equations as in Durian's model. Taking the Laplace transform with respect to time and then Fourier transform with respect to space, the matrix equation 3.1.3 becomes

$$s\,[\mathrm{i}]-[\mathrm{i}_0]=-ik\,[\mathrm{i}]+[M]\,[\mathrm{i}] \tag{3.1.6}$$

Here, "s" is the Laplace time variable and [i] is the matrix formed from transformed intensities.

$$[\mathrm{i}] = \begin{pmatrix} \mathrm{i}_{dp} \\ \mathrm{i}_{dm} \\ \mathrm{i}_{up} \\ \mathrm{i}_{um} \end{pmatrix} \tag{3.1.7}$$

Fourier transforming the spatial variable results with

$$[\mathrm{i}_0] = \begin{pmatrix} e^{-ikz_p} p_{ddpp} \\ e^{-ikz_p} p_{ddpm} \\ e^{-ikz_p} p_{dupp} \\ e^{-ikz_p} p_{dupm} \end{pmatrix} \tag{3.1.8}$$

where the source boundary conditions, Eq.3.1.9 are used. Here we considered a pulse of light deposited on the plane $z = zp = z_p(1-g)z_0$ at $t = 0$. Then the first scattering determines how the intensity is distributed to give

$$[I(z,0)] = \begin{pmatrix} I_{dp}(z,0) \\ I_{dm}(z,0) \\ I_{up}(z,0) \\ I_{um}(z,0) \end{pmatrix} = \begin{pmatrix} p_{ddpp}\delta(z-z_p) \\ p_{ddpm}\delta(z-z_p) \\ p_{dupp}\delta(z-z_p) \\ p_{dupm}\delta(z-z_p) \end{pmatrix} \tag{3.1.9}$$

The matrix $[M]$ may be brought into block diagonal form using matrix $[S]$ in a similarity form

$$[S] = \begin{pmatrix} 1 & 1 & 1 & 1 \\ 1 & 1 & -1 & -1 \\ 1 & -1 & 1 & -1 \\ 1 & -1 & -1 & 1 \end{pmatrix} \tag{3.1.10}$$

such that

$$[M'] = [S][M][S'] = \begin{pmatrix} 0 & -1-g-\kappa & 0 & 0 \\ -\kappa & 0 & 0 & 0 \\ 0 & 0 & 0 & -1-g_c-\kappa \\ 0 & 0 & -2-2\sigma-\kappa & 0 \end{pmatrix} \tag{3.1.11}$$

The similarity transform produces a new set of "intensities":

$$[\mathrm{i}'] = \begin{pmatrix} \mathrm{i}_{\mathrm{total}} \\ \mathrm{i}_{\mathrm{diff}} \\ \mathrm{i}_{\mathrm{polplus}} \\ \mathrm{i}_{\mathrm{polminus}} \end{pmatrix} = \begin{pmatrix} \mathrm{i}_{\mathrm{dm}} + \mathrm{i}_{\mathrm{dp}} + \mathrm{i}_{\mathrm{um}} + \mathrm{i}_{\mathrm{up}} \\ \mathrm{i}_{\mathrm{dm}} + \mathrm{i}_{\mathrm{dp}} - \mathrm{i}_{\mathrm{um}} - \mathrm{i}_{\mathrm{up}} \\ -\mathrm{i}_{\mathrm{dm}} + \mathrm{i}_{\mathrm{dp}} - \mathrm{i}_{\mathrm{um}} + \mathrm{i}_{\mathrm{up}} \\ -\mathrm{i}_{\mathrm{dm}} + \mathrm{i}_{\mathrm{dp}} + \mathrm{i}_{\mathrm{um}} - \mathrm{i}_{\mathrm{up}} \end{pmatrix} = [S][\mathrm{i}] \tag{3.1.12}$$

Here, $\mathrm{i}_{\mathrm{total}}$ stands for the total intensity independent of polarization, $\mathrm{i}_{\mathrm{polplus}}$ stands for the degree of polarization independent of propagation direction, $\mathrm{i}_{\mathrm{diff}}$ stands for the net direction of propagation independent of polarization and $\mathrm{i}_{\mathrm{polminus}}$ stands for the net direction of propagation and degree of polarization. Equation 3.1.6 may be written as

$$\begin{aligned} [S][N](s[\mathrm{i}] - [\mathrm{i}_0]) &= -ik[S][\mathrm{i}] + [\mathrm{S}][\mathrm{M}][\mathrm{S}^{-1}][S][\mathrm{i}] \\ &= -\mathrm{ik}[\mathrm{i}'] + [\mathrm{M}'][\mathrm{i}'] \end{aligned} \tag{3.1.13}$$

The matrix product $[S][N]$ introduces a minus sign and interchanges $\mathrm{i}_{\mathrm{total}}$ with $\mathrm{i}_{\mathrm{diff}}$ and $\mathrm{i}_{\mathrm{polplus}}$ with $\mathrm{i}_{\mathrm{polminus}}$ in $[\mathrm{i}]$. The resulting set of four equations for the intensities $[\mathrm{i}']$ is

$$\begin{pmatrix} e^{-ikz_p} g + (-1+g-s-\kappa)\,\mathrm{i}_{\mathrm{diff}} - ik\mathrm{i}_{\mathrm{total}} \\ e^{-ikz_p} - (s+\kappa)\mathrm{i}_{\mathrm{total}} - ik\,\mathrm{i}_{\mathrm{diff}} \\ g_c - e^{ikz_p} + (g_c - 1 - s - \kappa)\mathrm{i}_{\mathrm{polminus}} - ik\mathrm{i}_{\mathrm{polplus}} \\ (-1+2\sigma)e^{-ikz_p} - (2+s-2\sigma+\kappa)\,\mathrm{i}_{\mathrm{polplus}} - ik\mathrm{i}_{\mathrm{polminus}} \end{pmatrix} = 0 \qquad (3.1.14)$$

Now, the four-flux equations have separated into two sets of two equations with each set having the following form:

$$x_0 - (s-C)\bar{x} - ik\bar{y} = 0 \qquad (3.1.15.a)$$

$$y_0 - (s-D)\bar{y} - ik\bar{x} = 0 \qquad (3.1.15.b)$$

The first and third equations in matrix 3.1.14 are in the form of Eq.3.1.15.a while the second and fourth equations are in the form of Eq.3.1.15.b. For the first set of equations the (x_0, C) pair is $(e^{-ikz_p} g, g-1-\kappa)$ and $(e^{-ikz_p} g_c, g_c - 1 - \kappa)$ respectively. For the second set of equations the (y_0, D) pair is $(e^{-ikz_p}, -\kappa)$ and $((2\sigma-1)e^{-ikz_p}, 2\sigma - 2 - \kappa)$ respectively. For $z < z_p$, the inverse Fourier transforms of $\bar{x}$ and $\bar{y}$ are

$$\bar{x}_{less}(z,s) = C_1.e^{-\lambda z} + C_2.e^{\lambda z} + \left(((s-D)x_0 - y_0.\lambda).e^{\lambda(z-z_p)+ikz_p}\right)/2\lambda \qquad (3.1.16.a)$$

$$\bar{y}_{less}(z,s) = ((-C+s).C_1.e^{-\lambda z} + (C-s).C_2.e^{\lambda z})/\lambda + \left(((s-C)y_0 - x_0.\lambda).e^{\lambda(z-z_p)+ikz_p}\right)/2\lambda \qquad (3.1.16.b)$$

and for $z > z_p$

$$\bar{x}_{greater}(z,s) = C_1.e^{-\lambda z} + C_2.e^{\lambda z} + \left(((s-D)x_0 + y_0.\lambda).e^{-\lambda(z-z_p)+ikz_p}\right)/2\lambda \qquad (3.1.17.a)$$

$$\bar{y}_{greater}(z,s) = (-C+s).C_1.e^{-\lambda z} + (C-s).C_2.e^{\lambda z})/\lambda + \left(((s-C)y_0 + x_0.\lambda).e^{-\lambda(z-z_p)+ikz_p}\right)/2\lambda \qquad (3.1.17.b)$$

where $\lambda = \lambda_1 = \sqrt{(s - g + \kappa + 1)(s + \kappa)}$ for solution of the first two equations in matrix 3.1.14 or $\lambda = \lambda_2 = \sqrt{(s + 1 - g_c + \kappa)(s - 2\sigma + 2 + \kappa)}$ for solution of the last two equations in matrix 3.1.14. Using λ_1 in Eqs.3.1.15 yields two stream theory results where λ_1 and s can be expressed in terms of two-stream theory parameters, α and ω, and $\kappa \to 0$ respectively.

$$\lambda_1 = z_0 \alpha (1 - g) \tag{3.1.18}$$

$$s = z_0 \omega (1 - g) \text{ leading to } s = z_0{}^2 x (1 - g) \tag{3.1.19}$$

To determine the coefficients C_1 and C_2, new intensities that are computed by using Eqs.3.1.16 and Eqs.3.1.17 are introduced.

$$\bar{I}_{\downarrow less}(z, s) = (\bar{x}_{less} + \bar{y}_{less})/2 \tag{3.1.20.a}$$

$$\bar{I}_{\downarrow greater}(z, s) = (\bar{x}_{greater} + \bar{y}_{greater})/2 \tag{3.1.20.b}$$

$$\bar{I}_{\uparrow less}(z, s) = -(\bar{x}_{less} - \bar{y}_{less})/2 \tag{3.1.20.c}$$

$$\bar{I}_{\uparrow greater}(z, s) = -(\bar{x}_{greater} - \bar{y}_{greater})/2 \tag{3.1.20.d}$$

$\bar{I}_{\downarrow less}(z, s)$, $\bar{I}_{\downarrow greater}(z, s)$ represent the Laplace transform of either total downward intensity independent of polarization or degree of polarization in downward direction for $z < z_p$ and $z > z_p$, respectively. Similar definitions hold for $\bar{I}_{\uparrow less}(z, s)$ and $\bar{I}_{\uparrow greater}(z, s)$.

3.2 Results for DWS

3.2.1 Results for transmission

The evolution of the transmission of a pulse in Laplace time is written as $T(s) = (1-R)\bar{I}_{\downarrow greater}(\tilde{h}, s)$ where R is the average reflection probability of the diffusing photons and $\tilde{h} = \tilde{L}/(z_0(1-g)) = L/l_s$ is the scaled optical thickness. The dynamic transmitted pulse is calculated as in Eq.3.2.2 after finding coefficients C_1 and C_2 upon implementing the following boundary reflection relations:

$$\bar{I}_{\downarrow less}(0,s) = R\bar{I}_{\uparrow less}(0,s) \tag{3.2.1.a}$$

$$\bar{I}_{\uparrow greater}(\tilde{h}, s) = R\bar{I}_{\downarrow greater}(\tilde{h}, s) \tag{3.2.1.b}$$

$$T(s) = (1-R)\frac{\left((R-1)x_0 - (1+R)y_0\right)\lambda Cosh(z_p\lambda) + \left(D(1+R)x_0 - C(R-1)y_0 - s(x_0 + Rx_0 + y_0 - Ry_0)\right)Sinh(z_p\lambda)}{(R^2-1)2\lambda Cosh(\tilde{h}\lambda) + \left(C(-1+R)^2 + D(1+R)^2 - (1+R^2)2s\right)Sinh(\tilde{h}\lambda)}$$

(3.2.2)

It is appropriate to average Eq.3.2.2 by integrating over the penetration depth ratio. While taking the integral, $T(s)$ is multiplied by the term $e^{-z_p z_0}$ which represents the exponential decay of the incident beam with depth into the sample,

$$T'(C, D, R, x_0, y_0, \tilde{h}, \lambda, s) = \int_0^h T(s)e^{-z_p z_0} z_0 dz_p$$

$$= \frac{\left[x_0\lambda^2 - A' - \frac{1+R}{1-R}(B' - y_0\lambda^2)\right]z_0 e^{-\tilde{h}z_0}Sinh(\tilde{h}\lambda) + \left[A' + \frac{1+R}{1-R}(B' - (x_0+y_0){z_0}^2)\right]\lambda(1 - e^{-\tilde{h}z_0}Cosh(\tilde{h}\lambda))}{({z_0}^2 - \lambda^2)\left[\left(C + D\frac{(1+R)^2}{(1-R)^2} - 2\frac{(1+R^2)}{(1-R)^2}s\right)Sinh(\tilde{h}\lambda) - 2\lambda\frac{1+R}{1-R}Cosh(\tilde{h}\lambda)\right]}$$

(3.2.3)

where $A' = (C-s)y_0z_0$ and $B' = (D-s)x_0z_0$. For simplicity, the reflections of the incident, unscattered beam are ignored. In order to find the static transmission result, Eq.3.2.3 should be evaluated in the limit s goes the zero to find

$$T_p'(C,D,R,x_0,y_0,\tilde{h})$$

$$= \frac{\left[x_0CD - Cy_0z_0 - \frac{1+R}{1-R}(Dx_0z_0 - y_0CD)\right]z_0e^{-\tilde{h}z_0}Sinh\ (\sqrt{CD}\tilde{h}) + \left[Cy_0z_0 + \frac{1+R}{1-R}(Dx_0z_0 - (x_0+y_0)z_0^{\,2})\right]\sqrt{CD}(1-e^{-\tilde{h}z_0}Cosh\ (\tilde{h}\lambda))}{(z_0^{\,2}-CD)\left[\left(C+D\frac{(1+R)^2}{(1-R)^2}\right)Sinh\ (\sqrt{CD}\tilde{h}) - 2CD\frac{1+R}{1-R}Cosh\ (\sqrt{CD}\tilde{h})\right]}$$

.

(3.2.4)

3.2.1.a Result for total transmitted intensity independent of polarization

Substituting $(x_0, y_0, C, D) = (g, 1, g-1, 0)$ into $T(s)$ corresponds to the Laplace transformed transmitted pulse or the field autocorrelation function independent of polarization. When comparison to the two-stream representations is done by using equations 3.1.18 and 3.1.19, we find result Eq.3.2.5 to be exactly the same as the two-stream theory prediction, Eq.1.3.12.

$$T_{ip} = \frac{\left[1 + 2z_0\left(\frac{p - R(1-p)}{1-R}\right)\omega\right]Sinh(\alpha z p) + 2z_0\left(\frac{p + R(1-p)}{1-R}\right)\alpha Cosh(\alpha z p)}{\left(1 + 2z_0\frac{(1+R^2)}{(1-R)^2}\omega\right)Sinh(\alpha\tilde{L}) + 2z_0\left(\frac{1+R}{1-R}\right)\alpha Cosh(\alpha\tilde{L})} \qquad (3.2.5)$$

The index in T_{ip} stands for "independent of polarization". The relation between $\tilde{L}$ and $\tilde{h}$ is given by $\tilde{L} = z_0\tilde{h}(1-g)$.

Substitution of the same set of values, this time, in Eq.3.2.4 and neglecting absorption gives the static transmission probability, that is the four-stream prediction for DTS.

$$T_p' = \frac{1+g(z_0-1)+z_0\frac{1+R}{1-R}-e^{-\tilde{h}z_0}\left[1-g(1-z_0+\tilde{h}z_0)+z_0\frac{1+R}{1-R}+\tilde{h}z_0\right]}{\tilde{h}z_0(1-g)+2z_0\frac{1+R}{1-R}} \tag{3.2.6}$$

In the case of isotropic scattering, $g=0$, this reduces to

$$T_p' = \frac{1+z_e-e^{-\tilde{h}z_0}(1+z_e+\tilde{h}z_0)}{\tilde{h}z_0+2z_e} \tag{3.2.7}$$

which is in agreement with the DWS prediction Eq.1.2.19. In order to generate four-flux correlation function prediction for transmitted pulse independent of polarization, $g_{T_{ip}}$, $(x_0, y_0, C, D) = (g,1,g-1,0)$ values are used in Eq.3.2.3 and then the result is normalized by dividing Eq.3.2.6.

$$g_{T_{ip}}(x) = \frac{T'(g-1,0,R,g,1,\tilde{h},\lambda_1,s)}{T_p'} \tag{3.2.8}$$

The correlation function versus $(h^* z_0)^2 x$ is shown in figure 9 for four combinations of boundary reflectivity and scattering anisotropy. As seen from the plots, the correlation function decays faster when the scattering is anisotropic. It is because the light scatters more before leaving the sample. The influence of anisotropy becomes less for larger x and thicker samples. However, the effect of reflectivity persists even after the optical thickness has eliminated anisotropic effects. When multiple reflections are included, the static transmission becomes

$$T_p' = \frac{1+z_0\frac{1+R}{1-R}+g(z_0-1)-F\left[1+g(z_0+1)+h^* z_0+z_0\frac{1+R}{1-R}\right]+e^{-hz_0}(F-1)\left[1+g(z_0-1)+z_0\frac{1+R}{1-R}+h^* z_0\right]}{(1-F^2)h^* z_0+2z_0\frac{1+R}{1-R}} \tag{3.2.9}$$

where the probability for a photon to be reflected from the far boundary after crossing the sample without being scattered is expressed as $F = R_b.e^{-hz_0}$ where R_b is the reflection probability of ballistic photons and $h^* = \tilde{h}(1-g) = L/(l^* z_0)$.

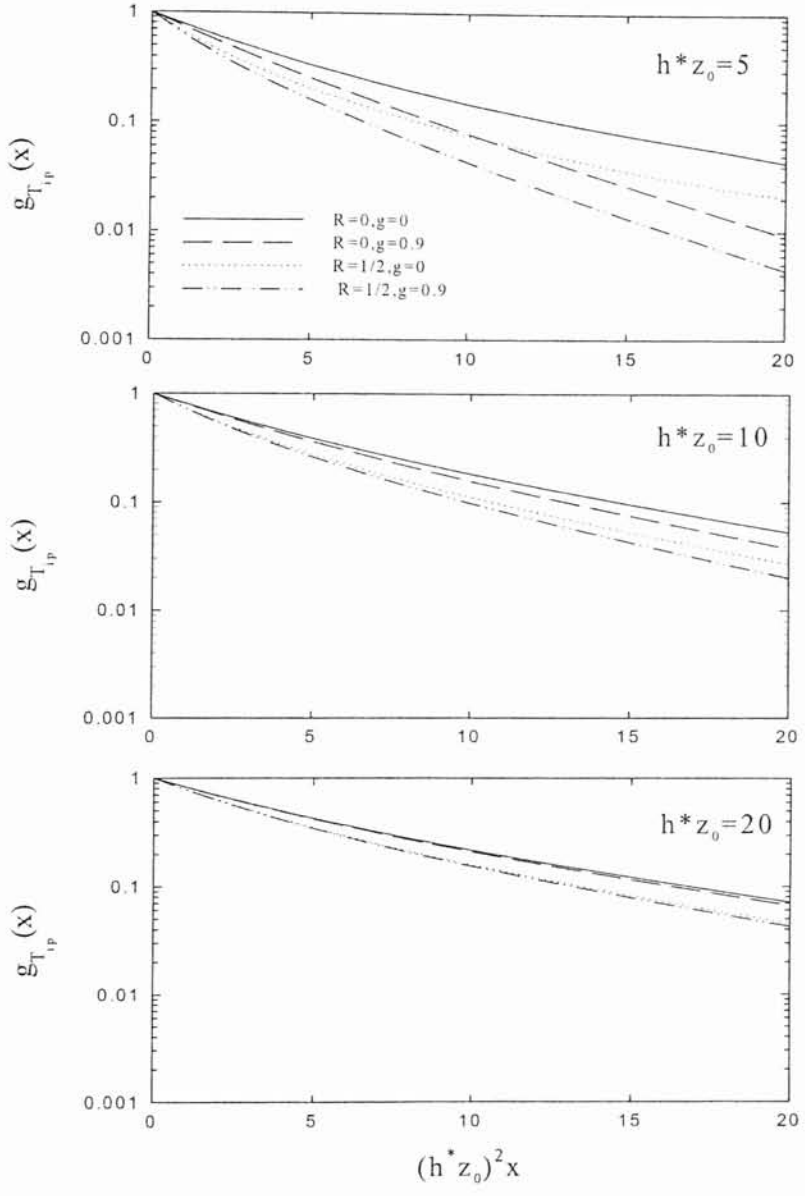

Fig.9- Four-stream predictions of Eq.3.2.8 for normalized electric field autocorrelation function for transmission independent of polarization through slabs of various thicknesses.

3.2.1.b Results for degree of polarization in the downward direction

Substituting $(x_0, y_0, C, D) = (g_c, 2\sigma - 1, g_c - 1, 2\sigma - 2)$ into $T(s)$ gives the degree of polarization in the downward direction:

$$T_{dp} = \frac{\left[\frac{1+R}{1-R} g_c (2\sigma - 2 - s) + (2\sigma - 1)(g_c - 1 - s)\right] Sinh(\lambda_2 z_p) - \left[g_c + \frac{1+R}{1-R}(2\sigma - 1)\right] \lambda_2 Cosh(\lambda_2 z_p)}{\left[(g_c - 1) - (2\sigma - 2)\left(\frac{1+R}{1-R}\right)^2 - 2\frac{1+R^2}{(1-R)^2} s\right] Sinh(\lambda_2 h) - 2\frac{1+R}{1-R}\lambda_2 Cosh(\lambda_2 h)} \tag{3.2.10}$$

The index in T_{dp} stands for "degree of polarization". In order to compute the degree of polarization of the light transmitted by the scattering medium for incident linearly and circularly polarized light, we should define the polarization parameter, δ. Experimentally, when a sample is illuminated by linearly polarized light, an analyzer is used to detect the scattered light whose polarization is either parallel or perpendicular to the incident light. In four-flux theory, we will take δ as 1 for parallel polarization and as –1 for perpendicular polarization. If the incident light is circularly polarized light, the scattered light can be either of the same helicity or of opposite helicity. When the incident and the scattered light are of the same helicity δ is 1 and δ is –1 if the other helicity is measured, for which incident and reflected photons are mirror symmetries of each other. Now, we are ready to write four-stream expression for the normalized autocorrelation function including polarization:

$$g_{T_{dp}}(x) = \frac{T'(g-1,0,R,g,1,\tilde{h},\lambda_1,s) + \delta T'(g_c - 1, 2\sigma - 2, R, g_c, 2\sigma - 1, \tilde{h}, \lambda_2, s)}{T_p{}'(g-1,0,R,g,1,\tilde{h}) + \delta T_p{}'(g_c - 1, 2\sigma - 2, R, g_c, 2\sigma - 1, \tilde{h})} \tag{3.2.11}$$

When δ =0, the polarization is neglected, and the above equation reduces to Eq.3.2.8 or the two-stream result for transmission, given in Eq.1.3.14. The plots of the results of

$g_{T_{dp}}(x)$ for circular polarization channels are shown in figure 10 and 11. These plots are all logarithm of the correlation function versus $(h^* z_0)^2 x$. The decay of the correlation function for different δ values for three different scaled optical thicknesses, $h^* z_0 = 5$, 10 and 20, can be seen in figure 10. The boundary reflectivity and scattering anisotropy are denoted by curve type: Solid line for $R = 0, g = 0$; long dash for $R = 0, g = 0.9$, dotted for $R = 1/2, g = 0$ and dash-dot-dot for $R = 1/2, g = 0.9$. Figure 10 exhibits polarization dependence of the autocorrelation function. It is seen that the decay of $g_{T_{dp}}(x)$ is more rapid when the incident and scattered light are of opposite helicity. This is better seen in the case of thin samples. As thickness increases the difference in the decay rate of $g_{T_{dp}}(x)$ for $\delta = 1$ and for $\delta = -1$ becomes less. Polarization dependence disappears as the thickness of the slab reaches $h^* z_0 = 20$. The same data is presented in figure 11 in a different fashion where it is easier to see how decay rate changes for different polarizations parameters, δ. The decay rate is greatest for $\delta = -1$ showing the greater contribution of long paths in opposite helicity channel. The anisotropy becomes less important for larger x and thicker samples. The fact that anisotropy increases with particle size leads to the conclusion that the form of correlation function depends on particle size. As well as depending on anisotropy, autocorrelation function also depends on the boundary reflectivity: Greater reflectivity causes quicker decay.

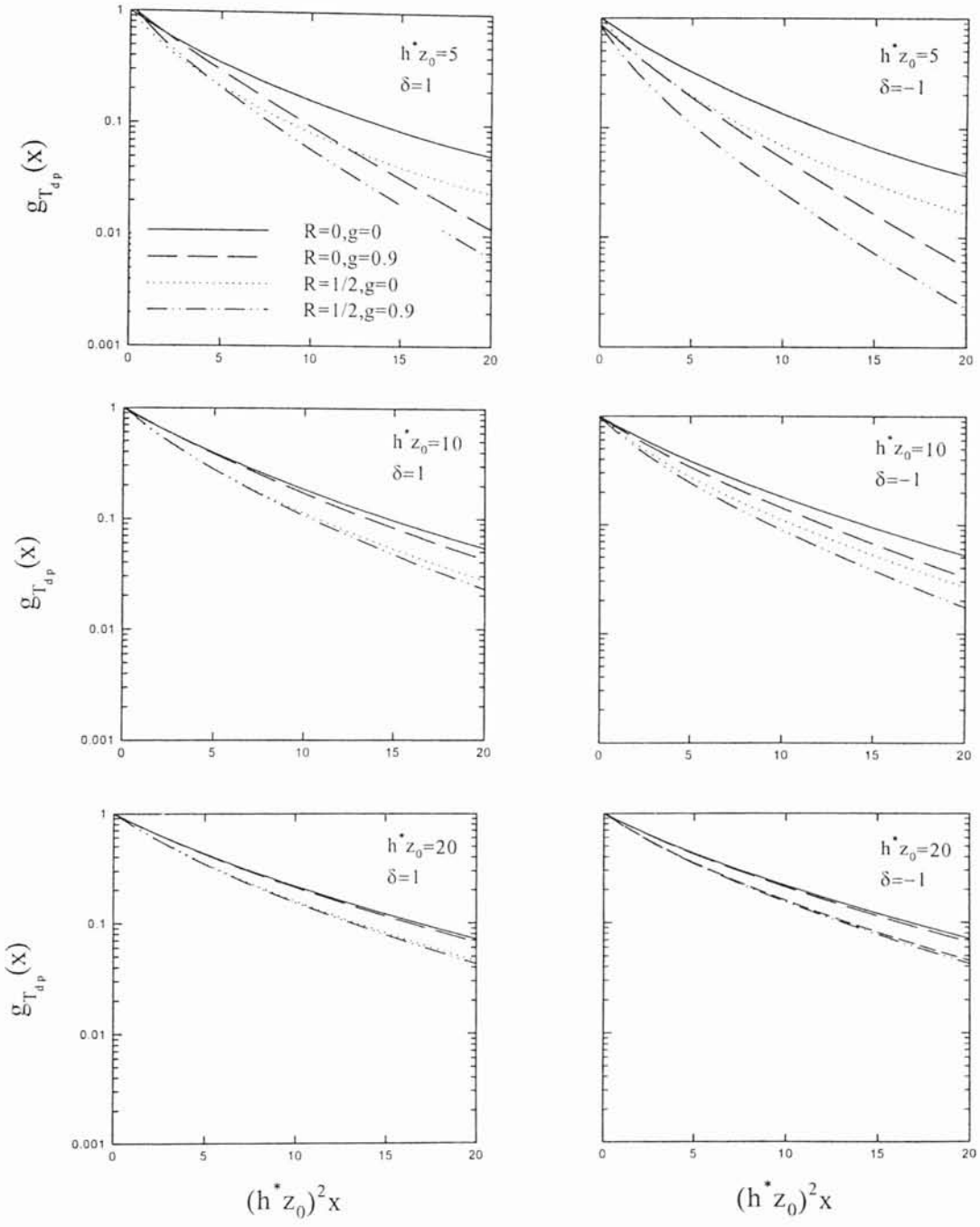

Fig.10- Four-stream predictions of Eq.3.2.11 for circularly polarized light through slabs of various thicknesses. The right (left) plots are for the case that the incident and the scattered light are of opposite (the same) helicity. Boundary reflectivity and scattering anisotropy are labeled.

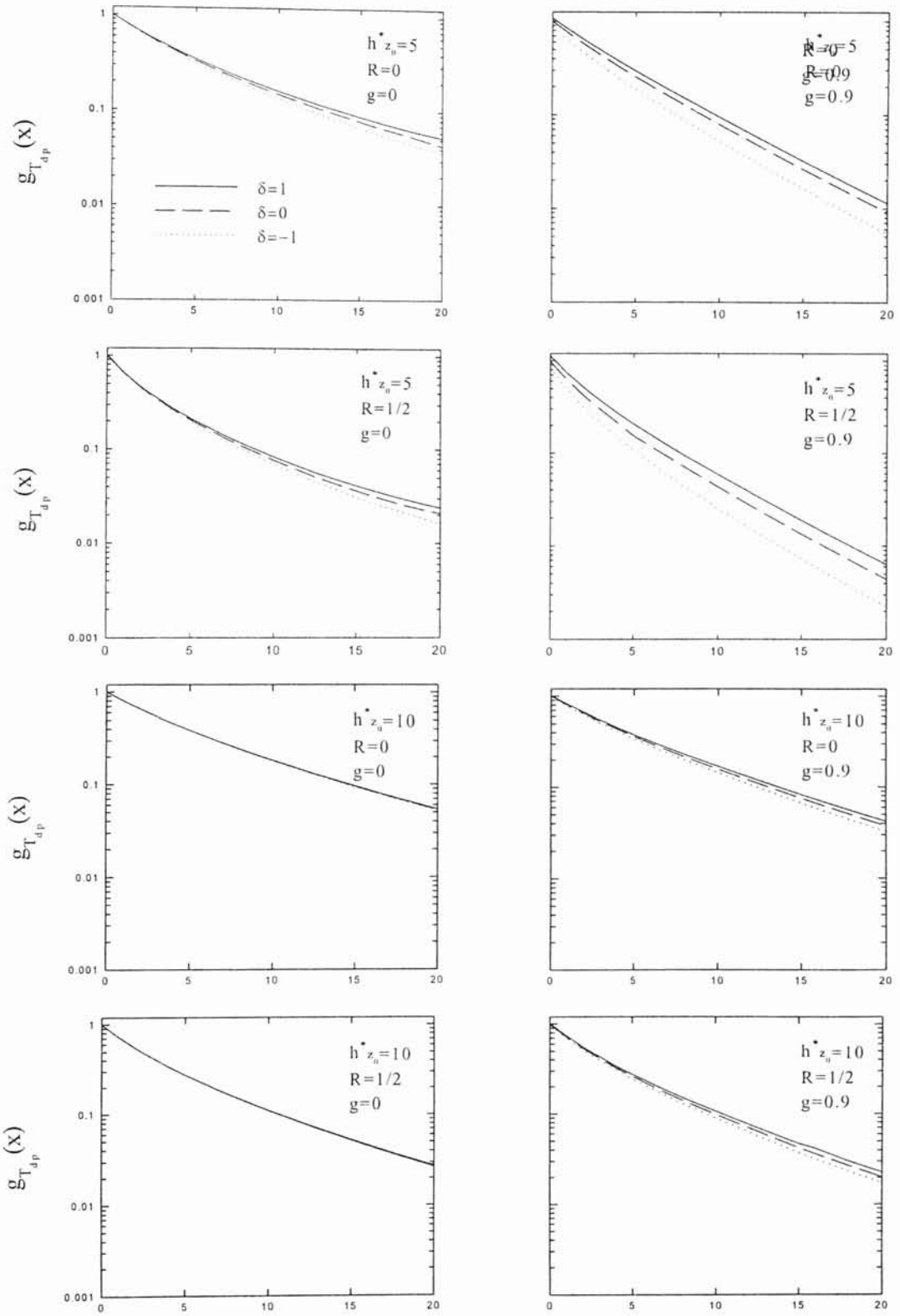
$g_{T_{dp}}(x)$
$h^* z_0 = 5$
R=0
g=0
δ=1
δ=0
δ=−1
$h^* z_0 = 5$
R=0
g=0.9
$h^* z_0 = 5$
R=1/2
g=0
$h^* z_0 = 5$
R=1/2
g=0.9
$h^* z_0 = 10$
R=0
g=0
$h^* z_0 = 10$
R=0
g=0.9
$h^* z_0 = 10$
R=1/2
g=0
$h^* z_0 = 10$
R=1/2
g=0.9
$(h^* z_0)^2 x$
$(h^* z_0)^2 x$

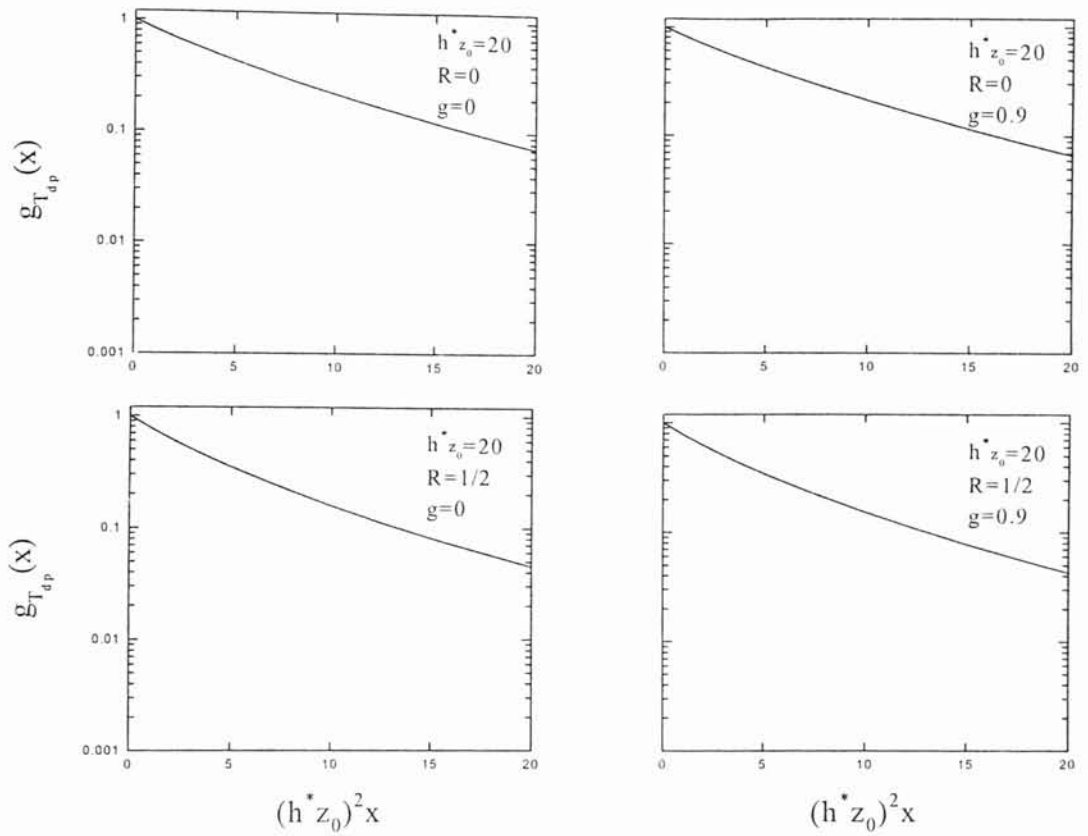

Fig.11- The dependence of transmission autocorrelation function on polarization in the case of circularly polarized incident light. Various thicknesses, boundary reflectivity and scattering anisotropy are labeled.

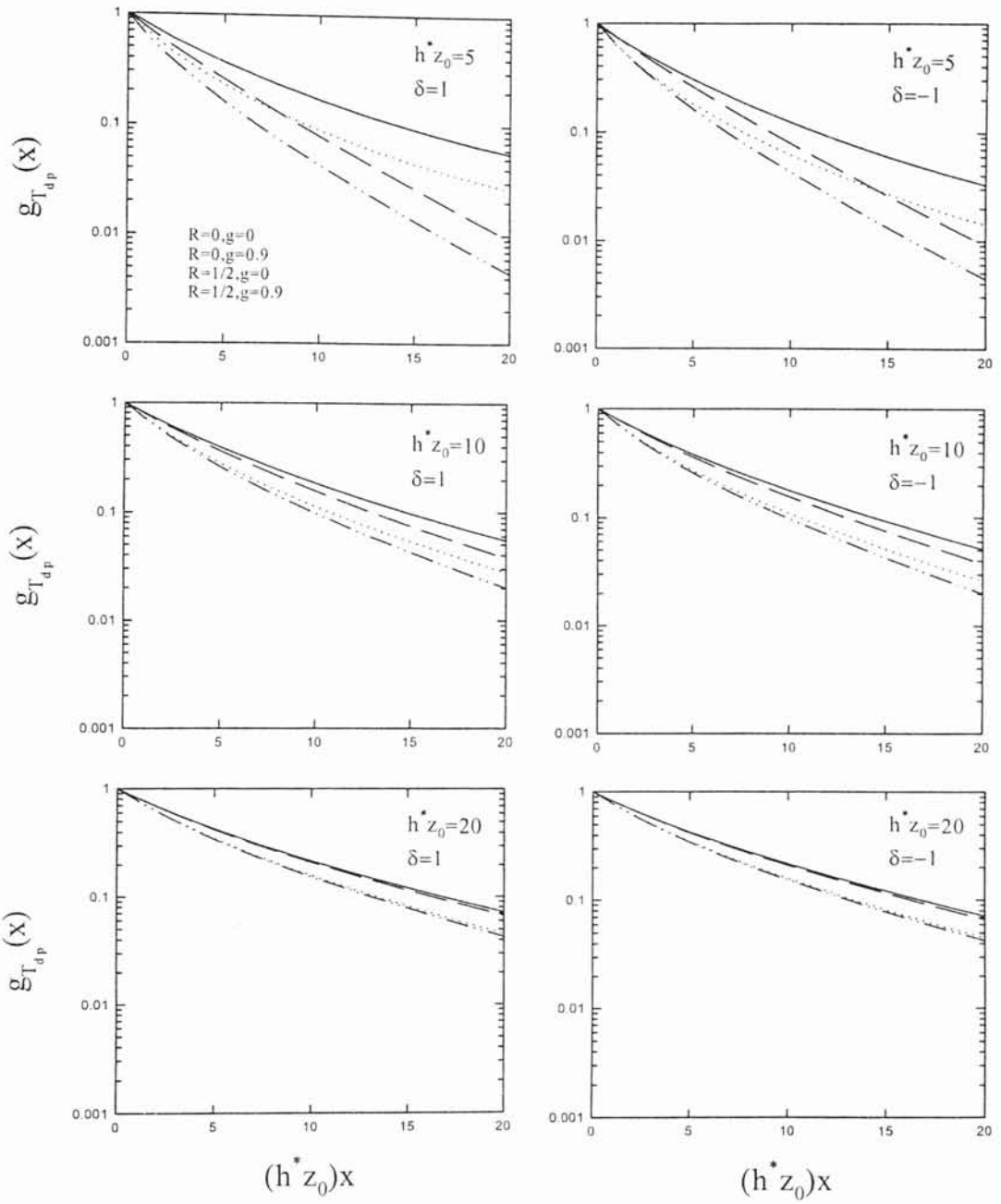

Fig.12- Four-stream predictions of Eq.3.2.11 for linearly polarized light through slabs of various thicknesses. The right plots are for perpendicular and the left plots are for parallel polarization. Boundary reflectivity and scattering anisotropy are labeled.

In figures 12 and 13,the behavior of the autocorrelation function is presented, this time, for linear polarization. The decay of $g_{T_{dp}}(x)$ is manifested again for different δ values and three different scaled optical thicknesses. The decay rate is greater for perpendicular polarization, i.e. the direction of the polarization of most of the scattered light is perpendicular to the incident light. However, as in the circular polarization case, the difference in the decay rate of $g_{T_{dp}}(x)$ for $\delta = 1$ and for $\delta = -1$ becomes less for thicker samples. For linearly polarized light, we can see the polarization dependence for just a slab of thickness of $h^{*}z_{0} = 5$. The polarization dependence remains to thicker samples when circular polarized light is used. This corresponds with the "rule of thumb" that $h^{*}z_{0} \geq 10$ for reliable measurements. When g gets larger, the circular polarization independence extends to much less than $h^{*}z_{0} \approx 10$. This should be checked experimentally.

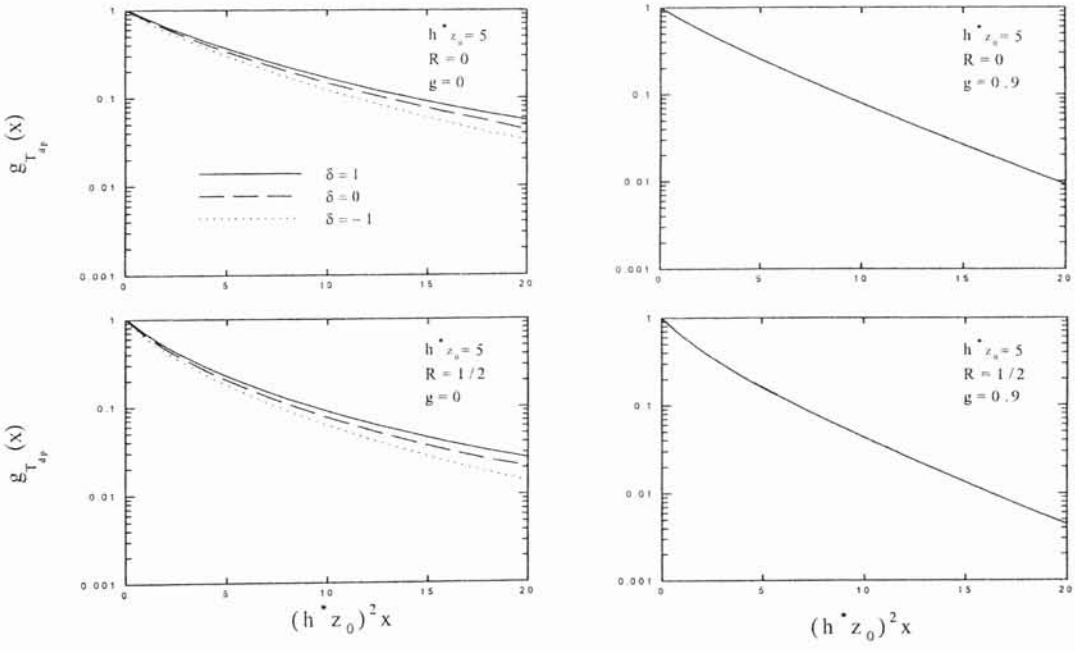

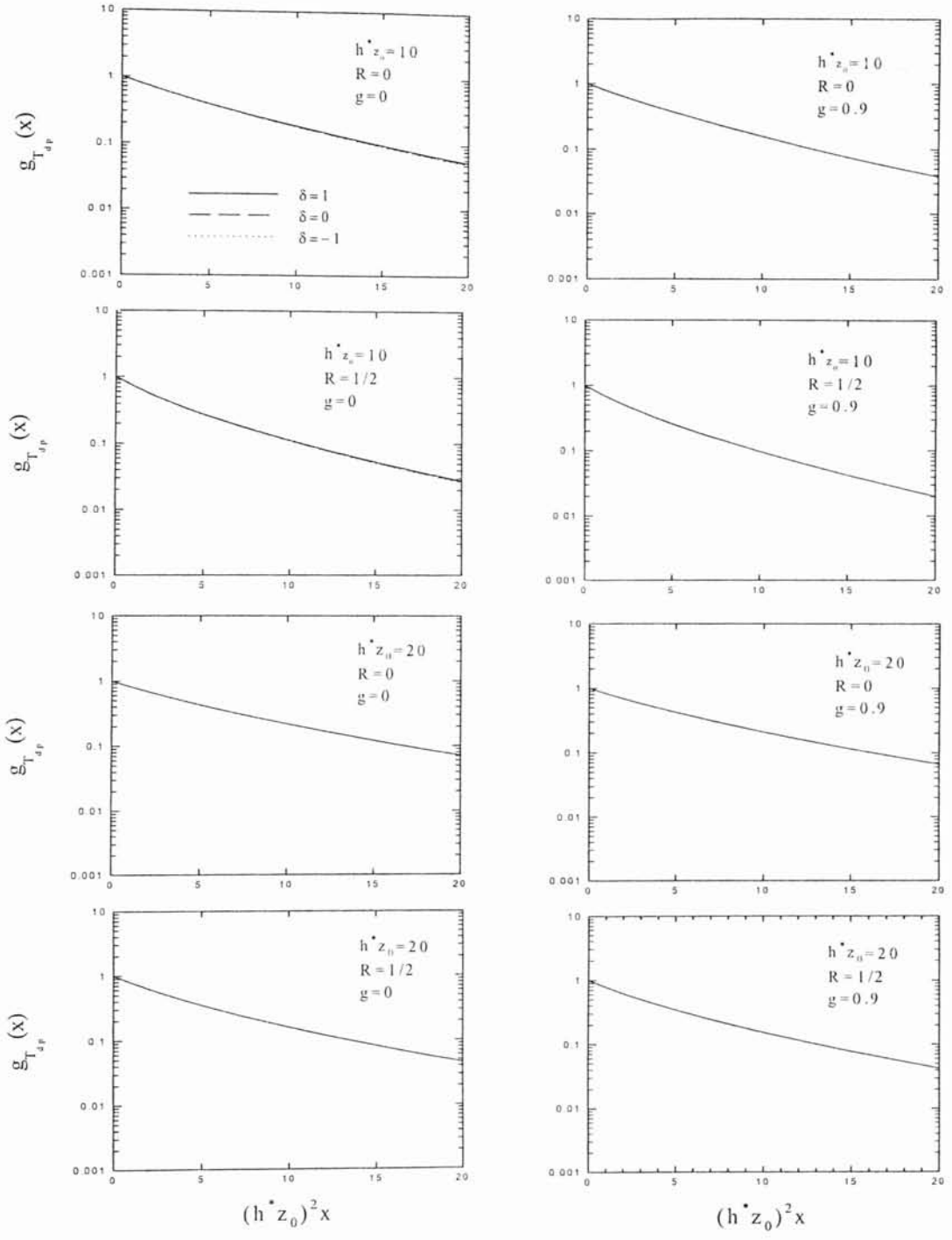

Fig.13- The dependence of transmission autocorrelation function on polarization in the case of linearly polarized incident light. Various thicknesses, boundary reflectivity and scattering anisotropy are labeled.

3.2.2. Results for backscattering

The evolution of backscattering in time is written as $B(s) = (1-R)\bar{I}_{\uparrow less}(0,s)$. Applying the boundary conditions, previously given in Eqs.3.2.1, the dynamic backscattered pulse is found as

$$B(s) = (-1+R)\frac{\left((R-1)x_0 + (1+R)y_0\right)\lambda Cosh\left((\tilde{h}-z_p)\lambda\right) + \left(B\ (1+R)x_0 + A\ (-1+R)y_0 - s(x_0 + Rx_0 - y_0 + Ry_0)\right)Sinh\left((\tilde{h}-z_p)\lambda\right)}{(R^2-1)2\lambda Cosh(\tilde{h}\lambda) + \left(A\ (R-1)^2 + B\ (1+R)^2 - (1+R^2)2s\right)Sinh(\tilde{h}\lambda)}$$

(3.2.12)

From Eq.3.2.12, we will try to get the autocorrelation function for a semi-infinite slab, for simplicity. For this purpose, $B(s)$ should be integrated over the penetration depth form 0 to ∞.

$$B'(C,D,R,x_0,y_0,\lambda,s) = \int_0^\infty B(s)e^{-z_p z_0} z_0 dz_p$$

$$= \frac{(y_0 - x_0)\lambda^2 z_0 + \left(x_0 {z_0}^2 - A' + \frac{1+R}{1-R}(B' - y_0 {z_0}^2)\right)\lambda - \left(A' + \frac{1+R}{1-R}B'\right)z_0}{({z_0}^2 - \lambda^2)\left[\left(C + D\frac{(1+R)^2}{(1-R)^2} - 2\frac{(1+R^2)}{(1-R)^2}s\right) - 2\lambda\frac{1+R}{1-R}\right]} \qquad (3.2.13)$$

3.2.2.a Results for total backscattered intensity independent of polarization

In order to generate the four-flux prediction for the backscattered pulse independent of polarization, the first set of (x_0, y_0, C, D) are $(g, 1, g-1, 0)$, respectively, should be substituted in $B(s)$. Comparison with the two-stream representation is done by using equations 3.1.18 and 3.1.19, we reach Eq.3.2.14 that exactly yields the two-stream theory prediction for the backscattered pulse, Eq.1.3.16.

$$B_{ip} = \frac{\left[1+2z_0\left(\frac{1-p(1+R)}{1-R}\right)\omega\right]Sinh\alpha(\tilde{L}-zp)+2z_0\left(\frac{1-p(1-R)}{1-R}\right)\alpha Cosh\alpha(\tilde{L}-zp)}{\left(1+2z_0\frac{(1+R^2)}{(1-R)^2}\omega\right)Sinh(\alpha\tilde{L})+2z_0\left(\frac{1+R}{1-R}\right)\alpha Cosh(\alpha\tilde{L})} \qquad (3.2.14)$$

To find the backscattered autocorrelation function without polarization, we simply evaluate $B' = (g-1,0,R,g,1,\lambda_1,s)$. The result will automatically equal to the normalized autocorrelation function, since in the limit $h \to \infty$, the normalization factor, $1-T_p'$, goes to 1.

$$g_{B_{ip}} = B'(g-1,0,R,g,1,\lambda_1,s) \qquad (3.2.15)$$

Four-flux predictions of Eq.3.2.15 are shown in the following graph for different boundary reflectivity and different anisotropy.

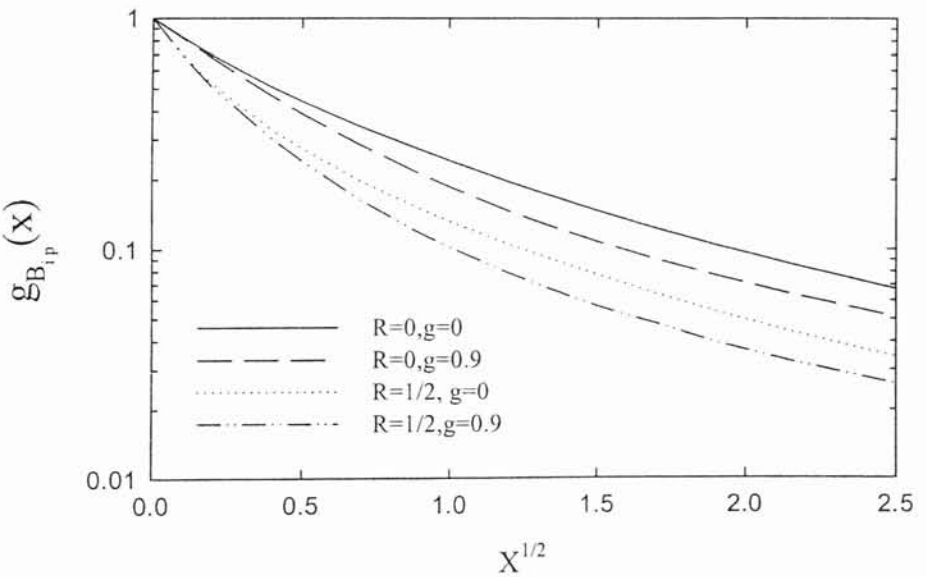

Fig.14- Four-stream predictions of Eq.3.2.15 for normalized electric field autocorrelation function for backscattering independent of polarization through slabs of various thicknesses.

3.2.2.b Results for degree of polarization in the upward direction

The substitution of $(x_0, y_0, C, D) = (g_c, 2\sigma - 1, g_c - 1, 2\sigma - 2)$ into $B(s)$ gives the degree of polarization in the backward direction, Eq.3.2.16.

$$B_{dp} = \frac{\left[(g_c-1)(2\sigma-1)-(2\sigma-2)g_c\frac{1+R}{1-R}-s\left((2\sigma-1)-g_c\frac{1+R}{1-R}\right)\right]Sinh\lambda_2(\tilde{h}-z_p)-\left[g_c-\frac{1+R}{1-R}(2\sigma-1)\right]\lambda_2 Cosh\lambda_2(\tilde{h}-z_p)}{\left[(g_c-1)+(2\sigma-2)\left(\frac{1+R}{1-R}\right)^2-2\frac{1+R^2}{(1-R)^2}s\right]Sinh(\tilde{h}\lambda_2)-2\frac{1+R}{1-R}\lambda Cosh(\tilde{h}\lambda_2)} \tag{3.2.16}$$

Taking the integral of B_{dp} should be taken from zero to infinity, we obtain:

$$B'(g_c-1,2\alpha-2,R,g_c,2\alpha-1,\lambda,s) = \int_0^\infty B_{dp}e^{-z_p z_0}dz_p \tag{3.2.17}$$

The four-flux expression that represents the observed polarization dependence of the autocorrelation function of backscattered light., is, then,

$$g_{B_{dp}}(x) = \frac{B'(g-1,0,R,g,1,\lambda_1,s)+\delta B'(g_c-1,2\sigma-2,R,g_c,2\sigma-1,\lambda_2,s)}{1+\delta\lim_{s\to 0}B'(g_c-1,2\sigma-2,R,g_c,2\sigma-1)} \tag{3.2.18}$$

Results for $g_{B_{dp}}(x)$ for four polarization channels are shown in figures 15 and 16. For isotropic scattering, helicity preserving channels decays faster. When the scattering particles are bigger, causing the scattering to be anisotropic, the effects of polarization differs. This time, opposite helicity channels have the greater decay rate. The helicity flip can also be observed in figure 17. For $g \to 0$ the circular polarization tends to flip on backscattering giving the slow decay for few scatterings. The preserving polarization sends the light deeper into the sample. For $g \to 1$ the polarization tends to be preserved on scattering, so the backscattering has the same helicity after one or more events. In the case of linear polarization, the decay rate is greater for perpendicular polarization for all four different combinations of boundary reflectivity and anisotropy. The fact that linear

character of polarization states is not affected that much by backscattering regardless of particle size can also be seen from figure 18. Linear polarization tends to be preserved. To change the polarization requires longer paths and hence more modulation.

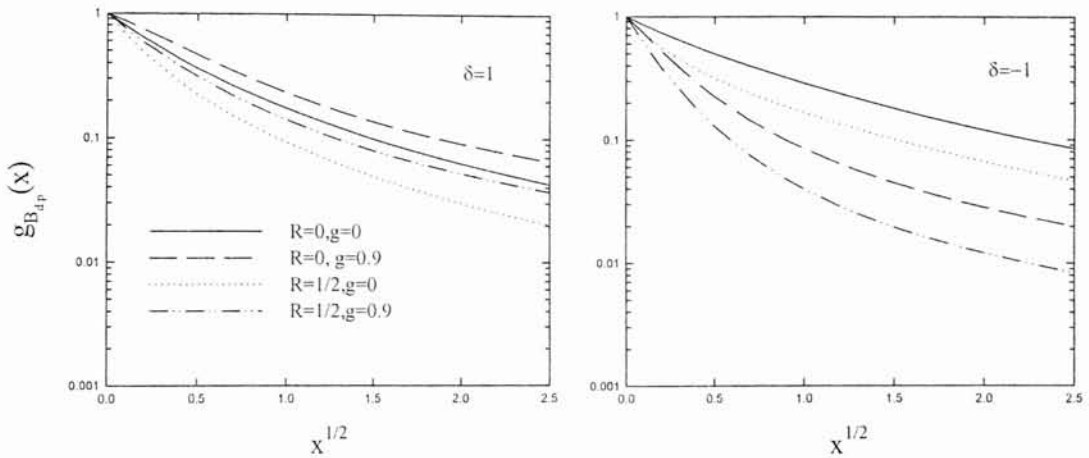

Fig.15- The decay of backscattered autocorrelation function for a semi-infinite slab for circular polarization channels. The left plot shows helicity preserving channel; the right plot shows opposite helicity channel.

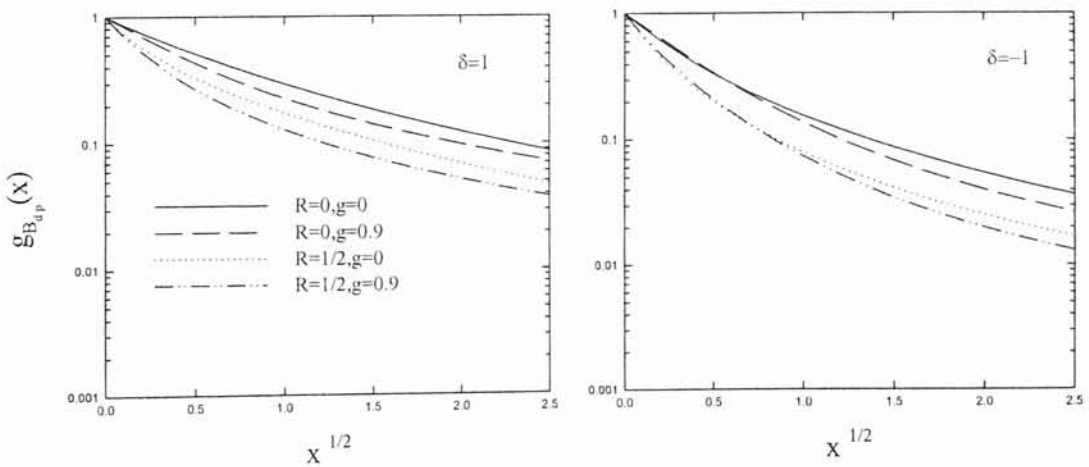

Fig.16- The decay of backscattered autocorrelation function for a semi-infinite slab for linear polarization channels. The left plot is for parallel; the right plot is for perpendicular polarization.

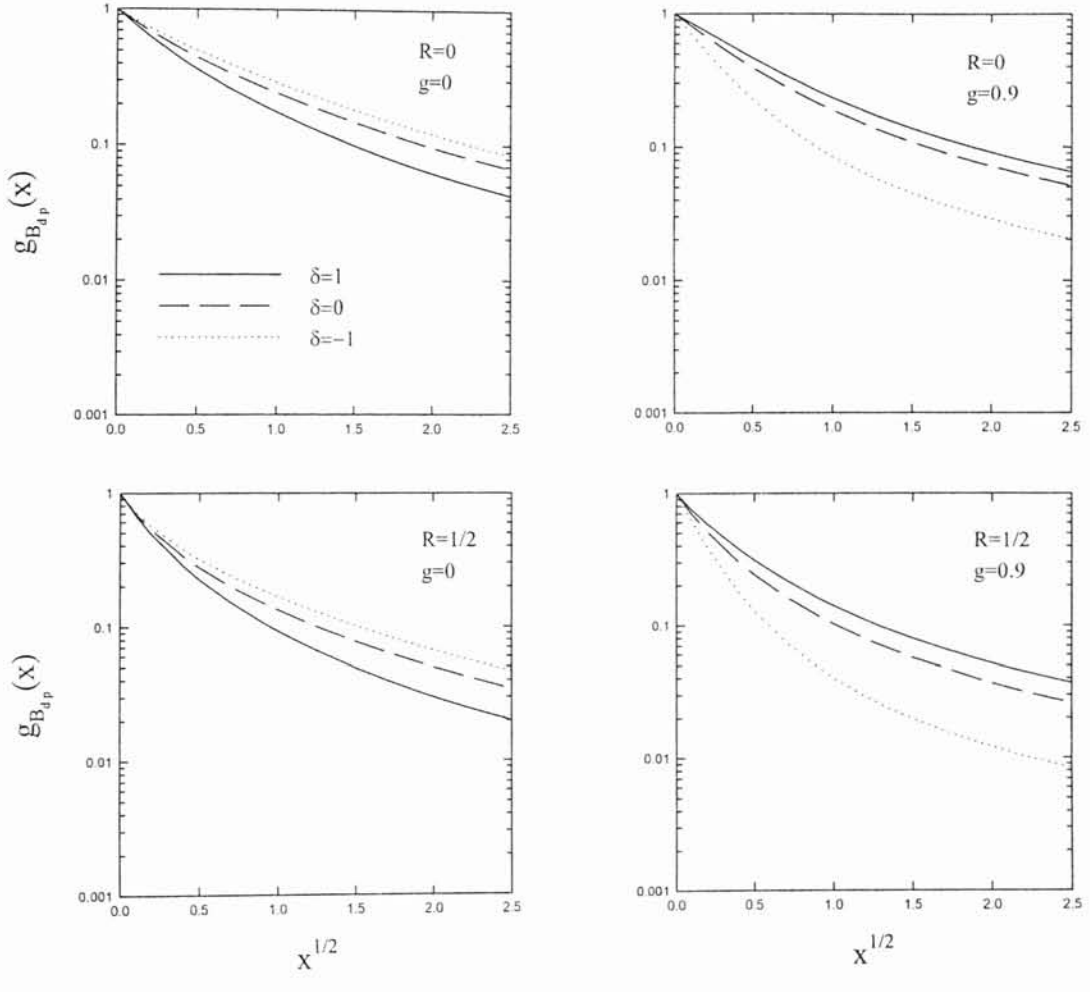

Fig.17- The dependence of backscattered autocorrelation function on polarization in the case of circularly polarized light. Various thicknesses, boundary reflectivity and scattering anisotropy are labeled.

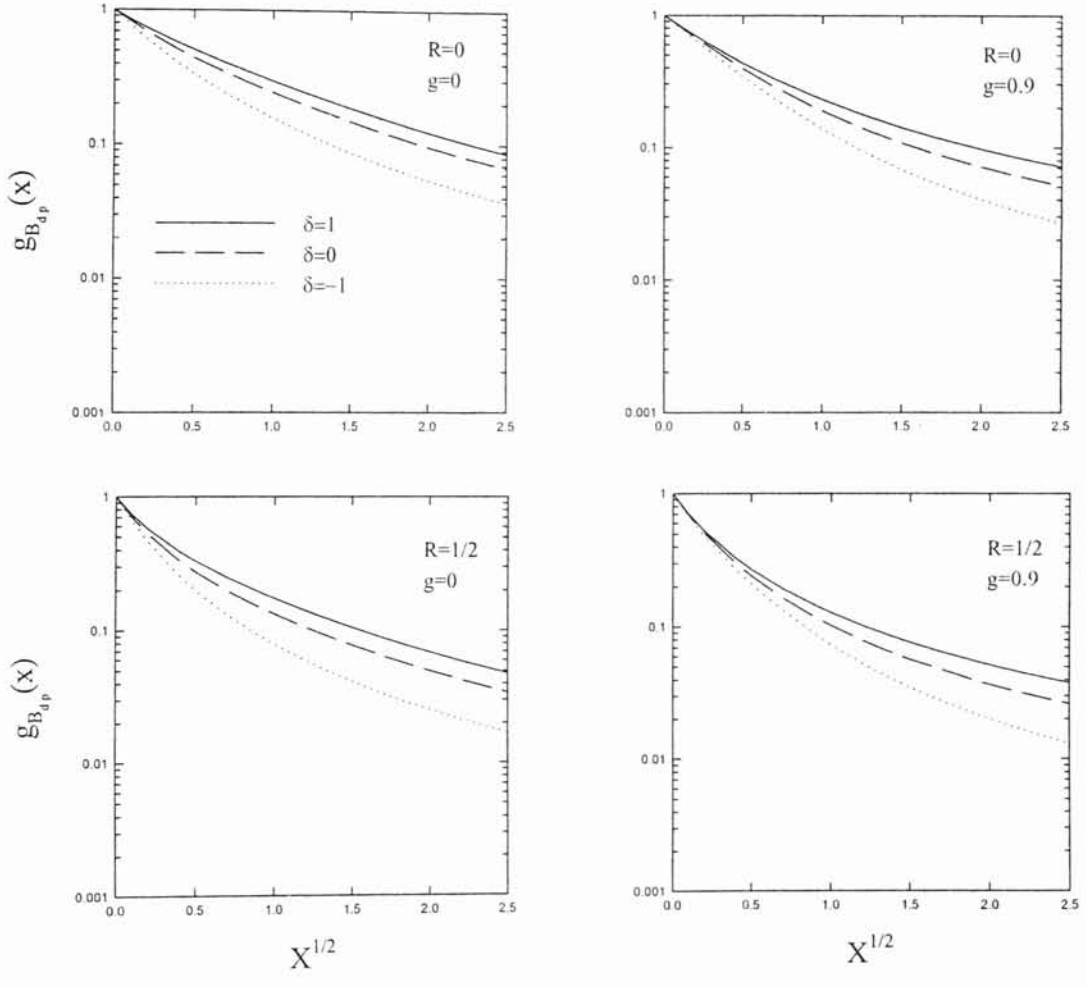

Fig.18- The dependence of backscattered autocorrelation function on polarization in the case of linearly polarized light. Various thicknesses, boundary reflectivity and scattering anisotropy are labeled.

Chapter 4

Discussion of results and conclusions

4.1 Comparisons of results

In the previous chapter, the results for dynamic four-stream theory for polarization have been presented. In this chapter, the linear and the circular polarization results will be compared for transmitted and backscattered light. A comparison of four-flux results for polarization with the existing experimental data will also be made. At the same time, agreement between four-stream and two-stream results will be mentioned.

4.1.a Comparisons of results for transmission

Including polarization in two-stream theory results in four-stream model. Therefore, at each step of our calculations, we have checked, if our results simplifies to two-stream results when polarization is neglected. It has been shown that the result of four-flux model for transmitted pulse independent of polarization, Eq.3.17 is exactly the same with the two-stream result, Eq.1.3.12. We have also showed when polarization is not considered the normalized autocorrelation function for degree of polarization in the downward direction, given by Eq.3.23 simplifies to Eq.3.20 which is in agreement with the two-stream result, Eq.1.3.14. The dependence of the correlation function on the polarization type and how polarization proceeds as the size of the particles increases from very small to very large are presented in figure 19 for various optical thicknesses.

For anisotropic case, the largest difference in decay rates is between two circular polarization states. As can be seen from the figure, the correlation function decays faster when the detector measures the helicity opposite from the incident light. This shows the greater contribution of long paths in opposite helicity channel. For isotropic case, the decay rate for incident linearly polarized light is greater than that for incident circularly polarized light. As the size of scattering particles gets larger, all polarization channels exhibit more rapid decay. However, as the thickness of the sample increases, all four channels show the same behavior, i.e. there is no dependence on polarization.

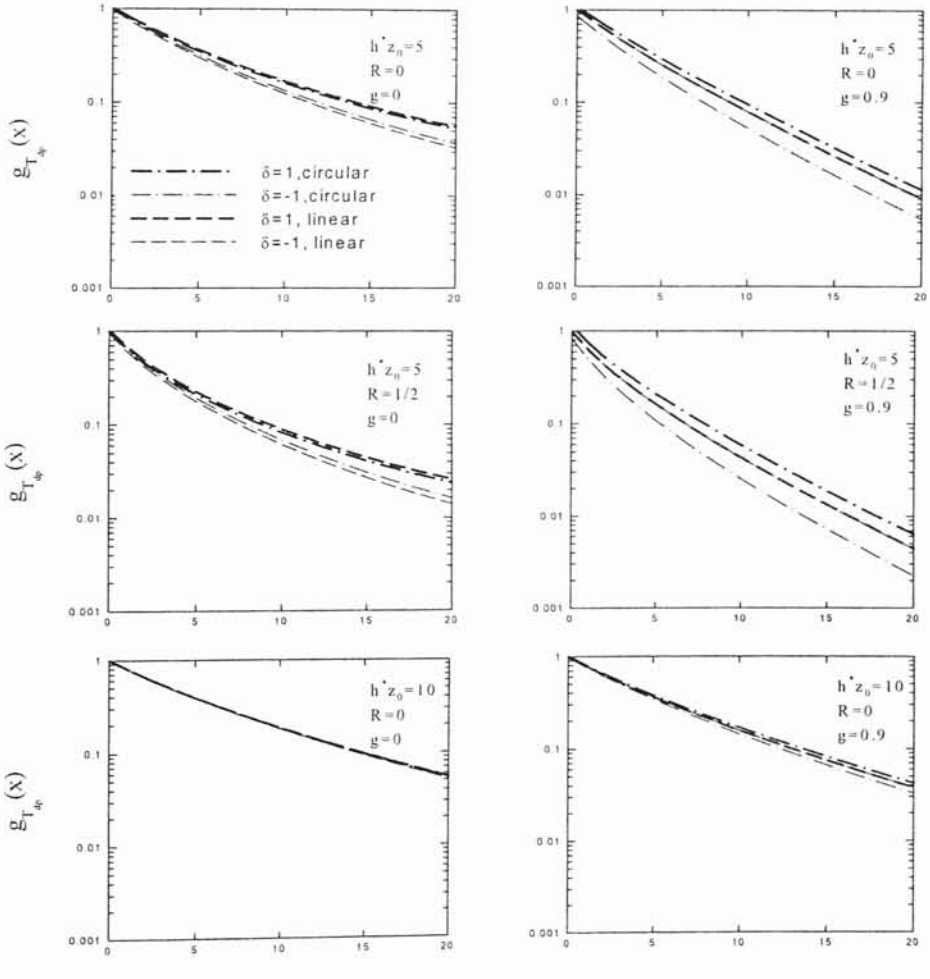

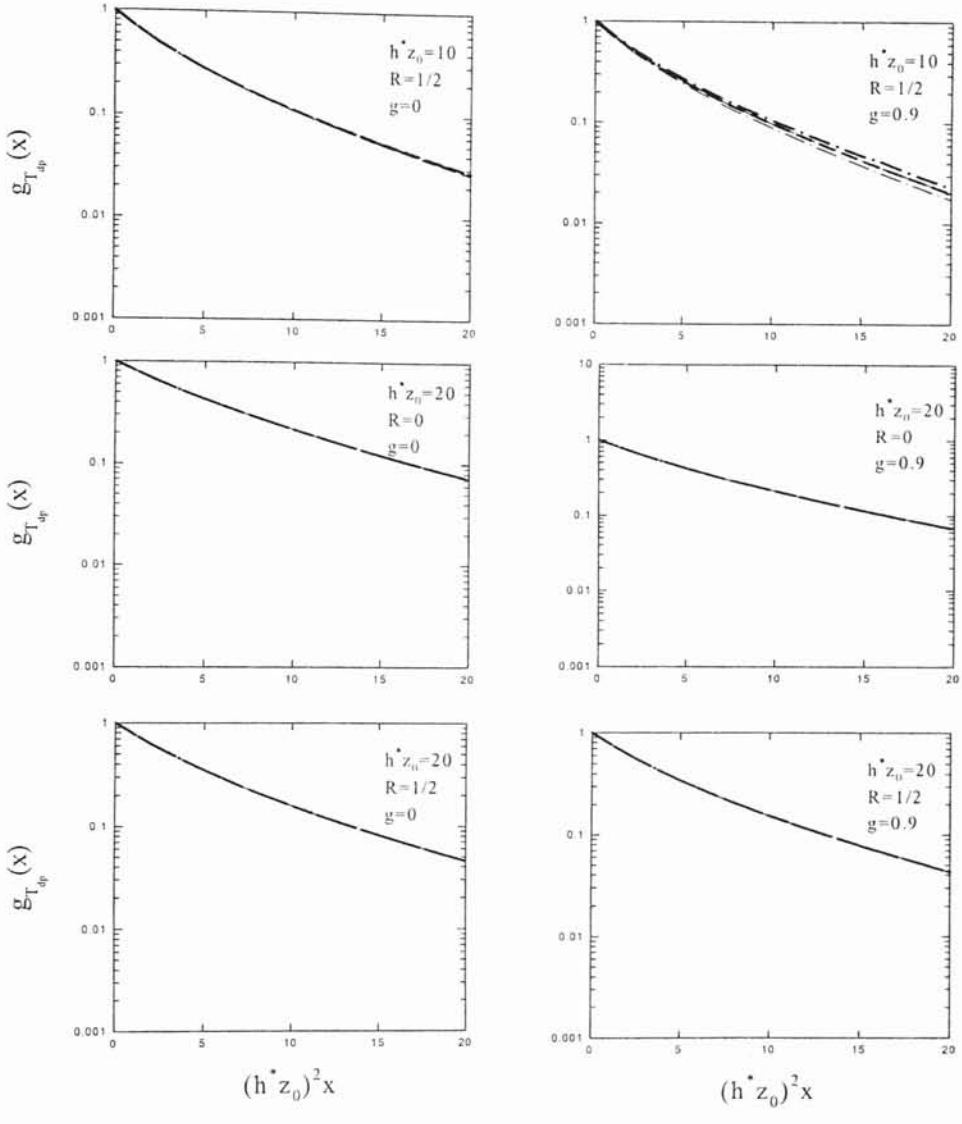

Fig.19- Four-stream predictions of transmission autocorrelation functions for four polarization channels for three different thicknesses. Four different combinations of boundary reflectivity and anisotropy are labeled.

A comparison of four-stream predictions with the experimental data for suspensions of polystryrene latex spheres in water can be done through comparison of the following figure. Figure 20 illustrates the four-stream static transmission results for degree of polarization, P, as a function of $h^* z_0$ for three different dimensionless size parameter ka values. A general equation for degree of polarization is given as

$$P = T_p{}'(g_c - 1, 2\alpha - 2, R, g_c, 2\alpha - 1, \tilde{h}) \tag{4.1}$$

The behavior of P, which is computed from Eq.4.1, is shown for three different ka values in figure 20.The curves all exhibit linear behavior in these plots. For Mie region, where particles are large compared to the wavelength, ka>1, the slopes depend strongly on the incident state of polarization. The slope for linearly polarized light is greater than the one for circularly polarized light. For ka~1, the slopes of these plots do not depend on the input polarization.

D. Bicout,C. Brosseau, A.S. Martinez and J.M. Schmitt studied numerically the depolarization behavior of light, propagating through a slab that is composed of uncorrelated polystryrene latex spheres, by using Monte Carlo simulation code [56,57]. They have also measured P experimentally with polystryrene latex spheres having diameters of 0.22,0.48 and 1.05 μm using a semiconductor laser emitting at 0.67 micrometer as the light source. These experimental values are compared with four-stream theory results in figure 21. For size parameter values of 1.23, 2.69,5.89 respectively. Four-stream results are in good agreement with the experimental results, especially for large ka values for circular polarization. However, the agreement is not good for linear polarization.

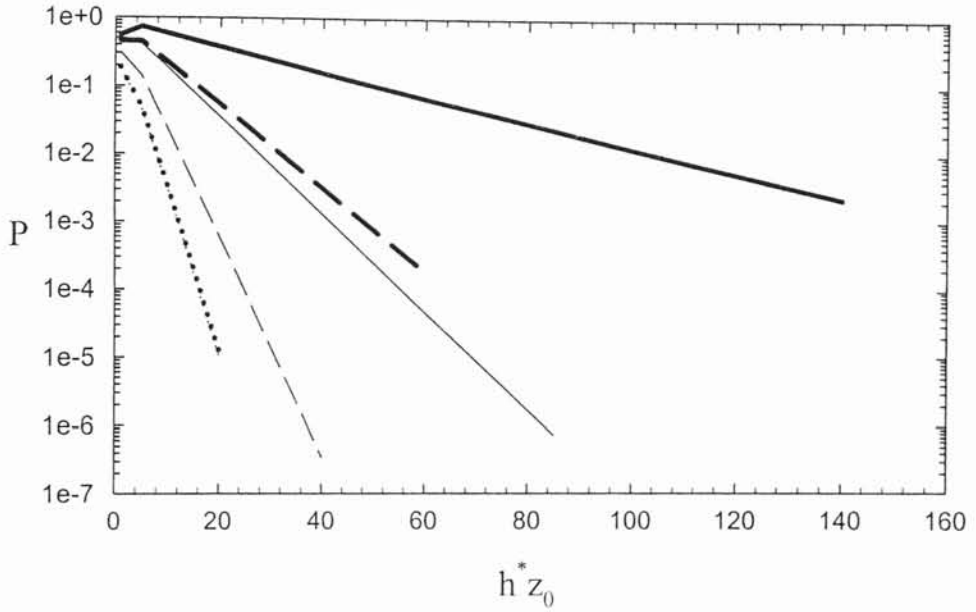

Fig.20- The degree of polarization vs. $h^* z_0$ for three different values of size parameter, ka. Different size parameters are signified by curve type: dots for ka=1.23; short dashes for ka=2.69; straight lines for ka=5.89. Thick curves are for circular; and thin curves are for linear polarization.

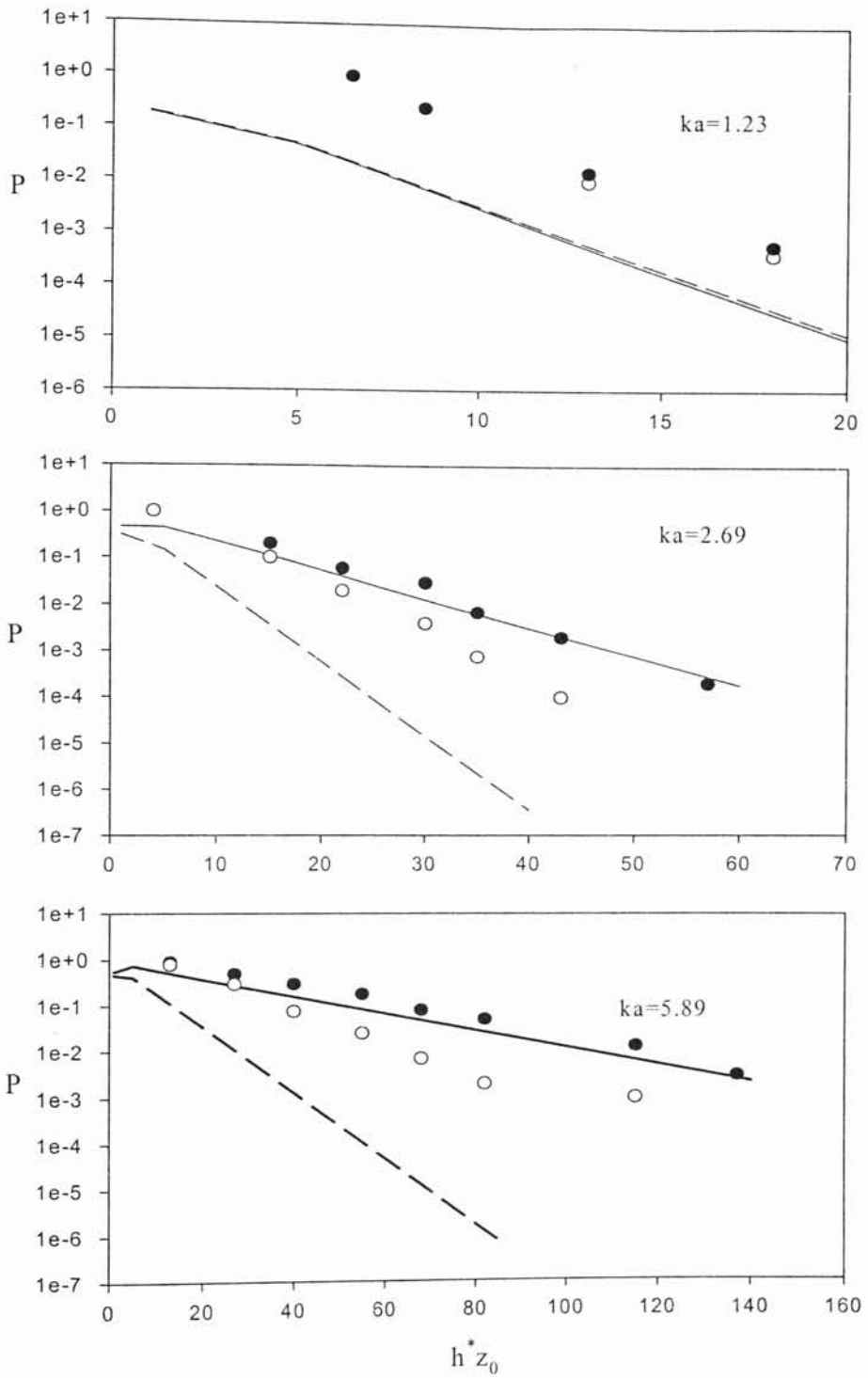

Fig.21- Comparison between the experimental values and the calculated values of degree of polarization P, for size parameters, ka=1.23,2.69,5.89. Solid (open) circles are experimental data points for circular (linear)polarization. Solid (dashed) lines are four-stream results for circular (linear) polarization.

4.2 Comparisons of results for backscattering

For the backscattering geometry, we have obtained dynamic backscattered pulse. It has been shown that the result of the four-flux model for the backscattered correlation function, Eq.3.26 is exactly the same with the two-stream result, Eq.1.3.16. When δ is taken zero, the normalized autocorrelation function for degree of polarization for backscattered light, given by Eq.3.30 also reduces to Eq.3.27 which is in agreement with the two-stream result Eq.1.3.18. The semilogarithmic plot of the backscattering autocorrelation function is shown in figure 22 for four polarization channels. The left plots are for isotropic cases while the right plots are for anisotropic cases. As can be seen from the figure, for isotropic scattering, the two linear polarization channels exhibit the largest difference in polarization, parallel polarization having a smaller slope. This shows that low order paths mostly preserves their incident polarization In the same manner, we can also conclude that high order paths changes the state of polarization to a high degree, resulting in a faster decay of the correlation function. There is also difference between circular channels. However, for circularly polarized light, low order sequences produce mostly backscattered light of opposite helicity. As a consequence, the opposite helicity channel decays slower than helicity preserving channel. While going from isotropic to anisotropic regime, backscattering, in a way, acts as an optical mirror, for circularly polarized states. Therefore, a reverse in the relative behavior of the circular polarization channels is observed, resulting the slope of helicity preserving channel to be larger. The greater contribution of short paths in the parallel polarization is still valid for linear polarization in the anisotropic regime.

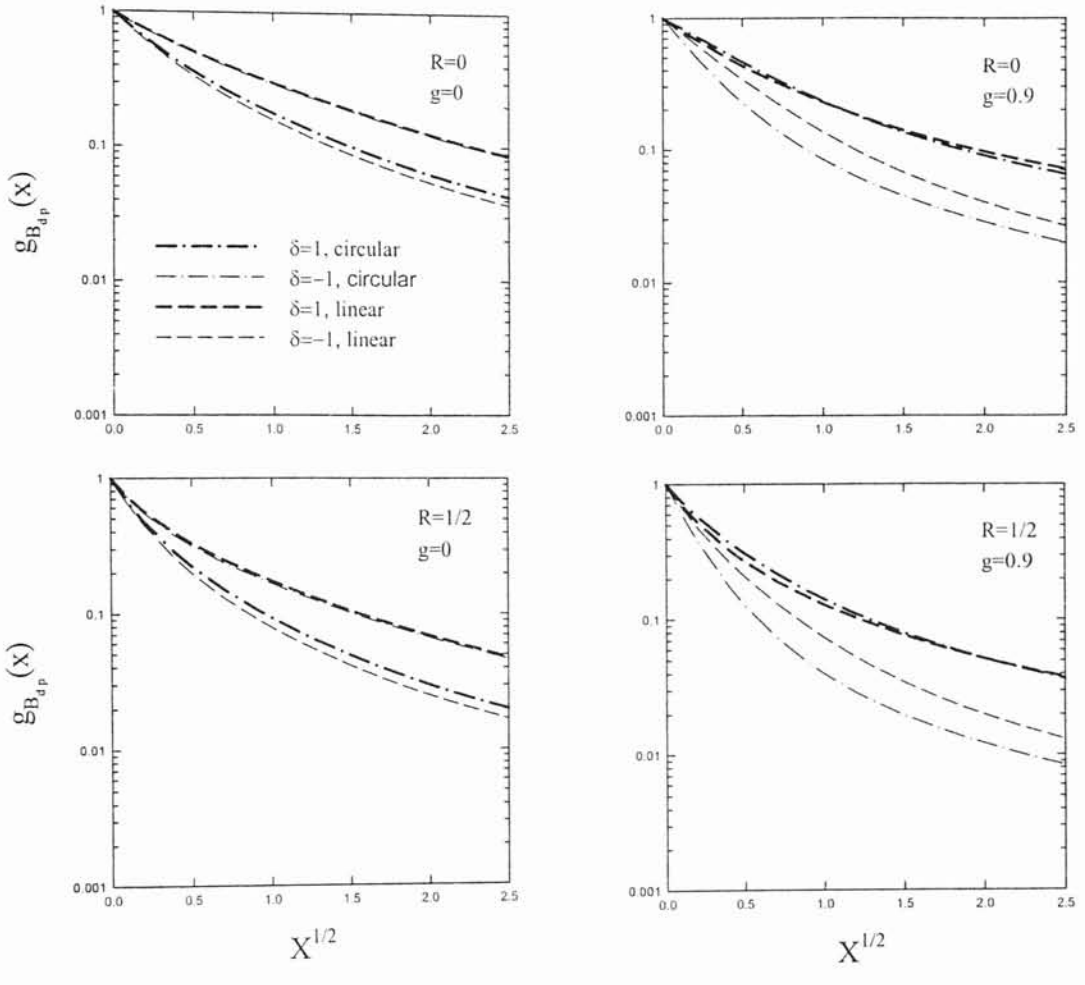

Fig.22- Four-stream predictions of backscattering autocorrelation functions for four polarization channels Four different combinations of boundary reflectivity and anisotropy are labeled.

The slopes of the plots in figure 22 are characterized by the parameter γ. As explained in section 1.2.c, γ appears as the coefficient of $\sqrt{x}$ when the short time expansion of $g_{B_{dp}}$, given in Eq.3.30, is taken. The four-flux prediction for γ is found as

$$\gamma = \frac{z_0 \dfrac{1+R}{1-R} + g(z_0 - 1) - 1}{1 + \delta N} \tag{4.2}$$

Here, N is

$$N=(g_c-1)(2\sigma-1)z_0^{\,2}-2g_c(\sigma-1)\frac{1+R}{1-R}z_0^{\,2}-\lambda_{20}^{\,2}(1+g_c-2\sigma)z_0-\lambda_{20}\left(g_c\frac{(z_0-1-R(3+z_0-4\sigma)}{1-R}-z_0\frac{1+R}{1-R}(2\sigma-1)-1\right)z_0$$

where $\lambda_{20}=\sqrt{2(\sigma-1)(g_c-1)}$. Taking the boundary reflectivity $R=0.004$, we now proceed to compare our four-flux results, for γ with the experimental data. The comparisons between Eq.4.2 for circular polarization states and measurements done by Mackintosh, Zhu, Pine and Weitz [58] are shown in figures 23 and 24, γ_+, showing the same helicity channel, and γ_- showing the opposite helicity. For small scattering particles $\gamma_- < \gamma_+$ while for large particles where forward scattering dominates $\gamma_- > \gamma_+$. The dependence of γ on particle size for two linear polarization types is illustrated in figures 25 and 26. Both four-flux model predictions and experimental measurements done by D.J. Pine, D,A,Weitz, J.X.Zhu and E. Herbolzheimer [11] are shown for slope of parallel polarization $\gamma_{\|}$ in figure 25. The similar comparison is shown for the slope of perpendicular polarization $\gamma_{\perp}$ in figure 26.

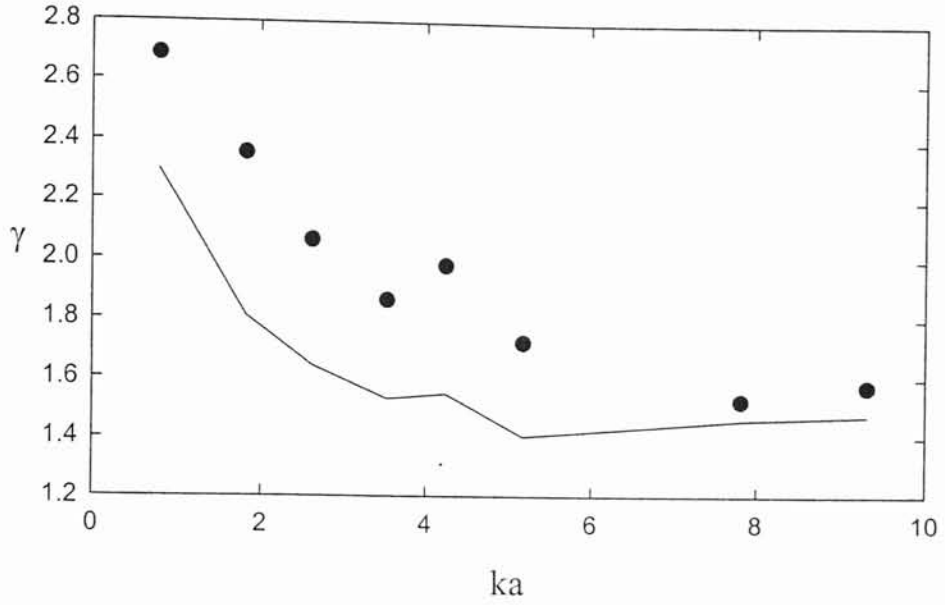

Fig.23- Comparison between the experimental value and the calculated value from four-stream theory of γ_+. The experimental data points are shown by solid circles and four-stream results are shown by solid line.

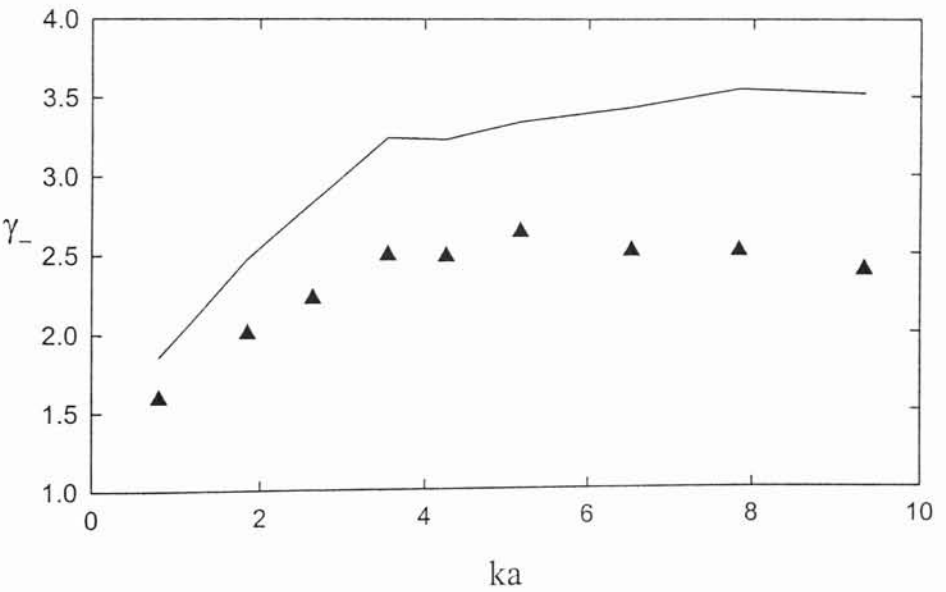

Fig.24- Comparison between the experimental value and the calculated value from four-stream theory of γ_-. The experimental data points are shown by solid circles and four-stream results are shown by solid line.

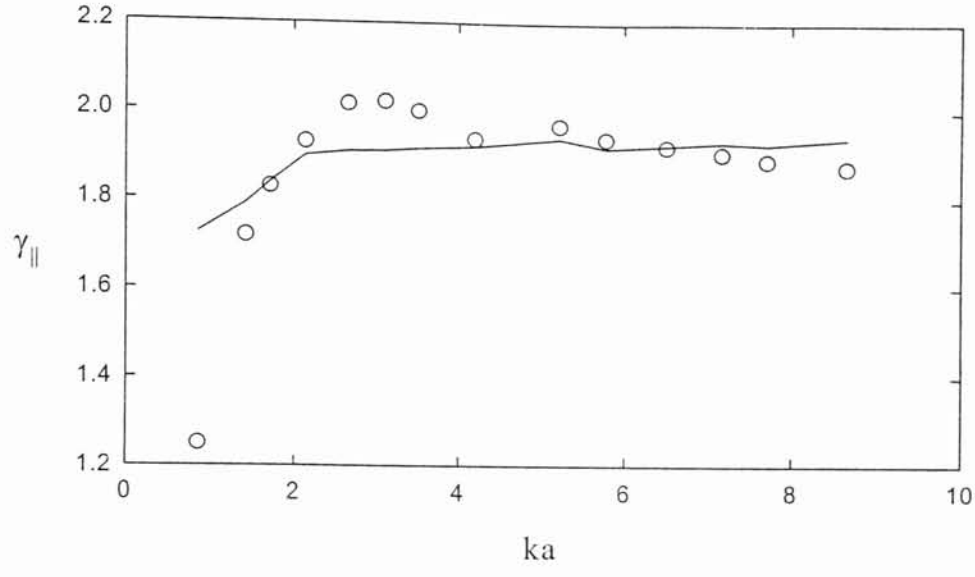

Fig.25- Comparison between the experimental value and the calculated value from four-stream theory of $\gamma_{\|}$. The experimental data points are shown by open circles and four-stream results are shown by solid line.

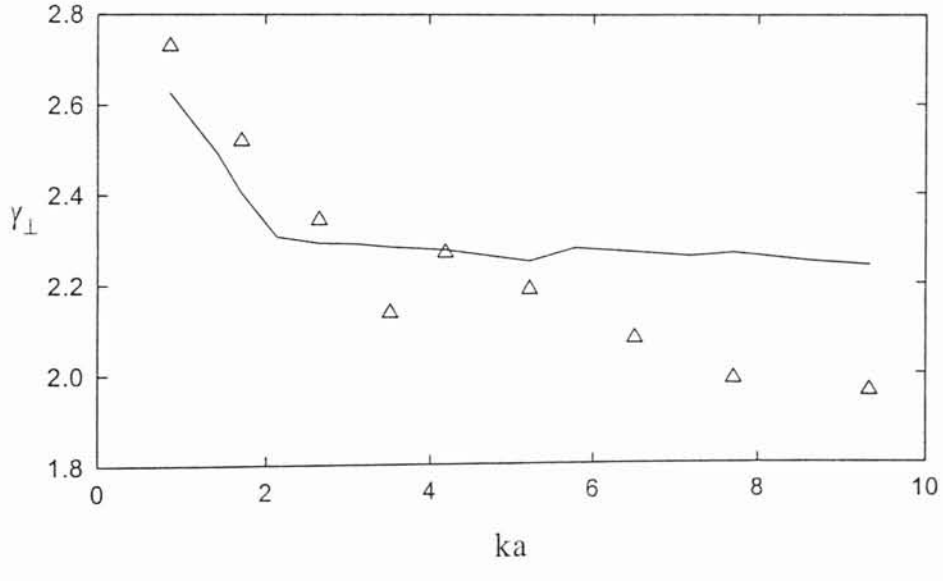

Fig.26- Comparison between the experimental value and the calculated vaue from four-stream theory of $\gamma_{\perp}$. The experimental data points are shown by open triangles and four-stream results are shown by solid line.

4.3 Conclusions

The objective of this research is to model for the observed polarization dependence in the behavior of transmitted or backscattered light, from an optically dense random medium. Satisfactory agreement of four-stream results with the two-stream results has been found when polarization is neglected, as mentioned previously. Thus, the achievements of two-stream theory are true for four-stream theory, as well: The results apply to arbitrary slab thickness, scattering anisotropy and boundary reflectivity. The improvement achieved by four –stream theory over two-stream theory is that, four-stream results include the type of polarization of incident and multiply scatted light. In order to validate our theoretical approach to polarization dependent scattering, we have compared our results with recent experimental data. The agreement between the measurements for static transmission with circularly polarized light and four-stream theory is good. However, for linearly polarized light, we observe a noticeable failure when compared with the data. Presumably this failure is related to the more ambiguous definitions of the microscopic parameters σ and g_c for linear polarization. Other formulations merit testing. For backscattering, there is reasonable agreement given the fact that neither two nor four stream theories produce the exact analytical form seen experimentally.

Our results can be used in multiple light scattering experiments that encounter the effects of multiple scattering on a polarized beam, thereby, allows one to probe the structure and dynamics of medium.

Bibliography

[1] C.F.Bohren, *Multiple Scattering of Light and some of its Observable Consequences*, Am. J. Phys. 55,6, June (1987)

[2] A. Ishimaru, *Wave Propagation and Scattering in Random Media*, Vols.1 and 2, Academic Press, New York (1978)

[3] S. Chandrasekhar, *Radiative Transfer*, Dover, New York (1960)

[4] Y.N. Barabanenkov, *On the Spectral Theory of Radiation Transport Equations*, Soviet Physics JETP 29, 4, 679 (1969)

[5] V. Twersky, *On Propagation in Random Media of Discrete Scatterers*, Proceedings of the American Mathematical Society Symposium on Stochastic Processes in Mathematical Physics and Engineering, Vol.16, American Mathematical Society, Providence, RI, 84 (1964)

[6] K. Furustu, *Multiple Scattering of Waves in a Medium of Randomly Distributed Particles and Derivation of the Transport Equation*, Radio Science 10, 1, 29 (1975)

[7] E. Wolf , *New Theory of Radiative Energy Transfer in Free Electromagnetic Fields*, Phy. Rev. D 13, 4, 869 (1976)

[8] D.J Pine, D. A. Weitz, G. Maret and P.E. Wolf, E. Herbolzheimer, and P. M. Chaikin, *Dynamic Correlations of Multiply Scattered Light*, In Scattering and Localization of Classical Waves in Random Media, Ed. P. Sheng, World Scientific, Singapore (1990)

[9] D. A. Weitz and D. Pine, *Diffusing-wave spectroscopy: dynamic light scattering*, Ed. Wyn Brown, Oxford Unv. Press, Oxford, England, UK (1993)

[10] D. J. Durian, *Penetration Depth of Diffusing-Wave Spectroscopy*, Appl. Opt. 34, 30 7100 (1995)

[11] D.J. Pine, D.A. Weitz, J. X. Zhu and E. Herbolzheimer, *Diffusing Wave Spectroscopy : dynamic light scattering in the multiple scattering limit*, J. Phys. France 51, 2101 (1990)

[12] D.A. Weitz, J. X. Zhu, D.J. Durian, H. Gang and D.J. Pine, *Diffusing wave spectroscopy: the technique and some applications*, Phys. Scr. T49, 610 (1993)

[13] *Dynamic Light Scattering: Applications of Photon Correlation Spectroscopy*, Ed. R. Pecora, Plenum Press, NewYork (1985)

[14] G. Maret, P.E.Wolf, Z. Phys. B 65,409 (1987)

[15] P. D. Kaplan, A. G. Yodh, and D. F. Townsend, *Noninvasive Study of Gel Formation in Polymer-stabilized Dense Colloids Using Multiply Scattered Light*, J. Colloid Interface Sci. 155, 319 (1993)

[16] D. A. Weitz, D. J. Pine , P. N. Pusey, and R. J. A. Tough, *Nondiffusive Brownian Motion Studied by Diffusing-Wave Spectroscopy*, Phys. Rev. Lett. 63, 1747 (1989)

[17] X. Qiu, X. L. Wu, J. Z. Xue, D. J. Pine, D. A. Weitz, and P. M. Chaikin, *Hydrodynamic Interactions in Concentrated Suspensions*, Phys. Rev. Lett. 65, 516 (1990)

[18] A. Mertelj and M. Copic *Dynamic Light Scattering as a Probe of Orientational Dynamics in Confined Liquid Crystals*, Phys. Rev. E 61, 2, 1622 (2000)

[19] Drevenšek Olenik, M. Jazbinšek and M. Copic, *Dynamic Light Scattering at Optical-Field-Induced Freedericksz Transition in Nematic Liquid Crystal*, Mol. Cryst. Liq. Cryst. 329, 101 (1999)

[20] P. Stanislav and N. Patrick, *A Light Scattering Theory for Filled Diluted Polymer Solution under Flow*. J. Phys. France 5,1017 (1995)

[21] P. C. Hiemenz, *Light Scattering by Polymer Solutions in Polymer Chemistry: The Basic Concepts*, Chpt. 10, Pub. Marcel Decker Inc., New York (1984)

[22] A. Palmer, J. Xu, S.C. Kuo, and D. Wirtz, *Diffusing Wave Spectroscopy Microrheology of Actin Filament Networks*, Biophy. J. 76, 1063 (1999)

[23] B.J.Berne and R. Pecora, *Dynamic Light Scattering with Applications to Chemistry, Biology and Physics*, Wiley Interscience, NewYork (1976)

[24] W. F. Cheong, S. A. Prahl, and A. J. Welch, *A Review of the Optical Properties of Biological Tissues*, IEEE J. 26, 2166 (1990)

[25] B. C. Wilson, E. M. Sevick, M. S. Patterson, and B. Chance , *Time Dependent Optical Spectroscopy and Imaging for Biomedical Applications* ,IEEE J. 80, 918 (1992)

[26] A.H. Hielscher, J.R.Mourant, I.J. Bigio, *Influence of Particle Size and Concentration on the diffuse backscattered of Polarized Light from Tissue Phantoms and Biological Cell Suspensions.* Appl. Opt. 36, 125 (1997)

[27] J. H Page, M. L. Cowan and D. A. Weitz, *Diffusing Acoustic Wave Spectroscopy of Fluidized Suspensions*, Physica B 279, 130 (2000)

[28] G. Maret and P.E. Wolf, *Multiple Light Scattering from Disordered Media the Effect of Brownian Motion of Scatterers*, Phys Rev. B 65, 409 (1987)

[29] M. Rosenbluh , M. Hoshen, I. Freund and M. Kaveh, Phys. Rev. Lett. 58, 2754 (1987)

[30] M. J. Stephen, Phys. Rev. B 37,1 (1988)

[31] I. Freund, M. Kaveh, and M. Rosenbluh, Phys. Rev. Lett. 60, 1130 (1988)

[32] D.J Pine, D. A. Weitz, P. M. Chaikin, and E. Herbolzheimer, *Diffusing-wave Spectroscopy*, Phys. Rev. Lett. 60, 1134 (1988)

[33] S. O. Rice, *Mathematical Analysis of Random Noise in Noise and Stochastic Processes*, Ed. N. Wax, Dover, New York (1954)

[34] P. E. Wolf, G. Maret, E. Akkermans, and R. Maynard , J. Phys. France 49,63 (1988)

[35] L. Landau and E. M. Lifshitz, *Statistical Physics*, pg. 63, Permagon, Oxford (1980)

[36] J. X. Zhu, D.J. Pine and D. A. Weitz, Phys. Rev. A 44, 3948 (1991)

[37] P.A. Lemieux, M.U. Vera, and D.J. Durian, *Diffusing-light Spectroscopies Outside the Diffusive Limit: The influence of ballistic transport and anisotropic scattering*, Phys. Rev. E 57, 4498 (1998)

[38] D. J. Durian, Phys. Rev. E 50, 857 (1994)

[39] M. U. Vera and D. J. Durian, Phys. Rev. E 53, 3215 (1996)

[40] Dws.pdf or atla ref 16(?)

[41] P. D. Kaplan, M. H. Kao, A. G. Yodh, and D. J. Pine, Appl. Opt. 32, 3828 (1993)

[42] D.J Pine, D. A. Weitz, P. M. Chaikin, and E. Herbolzheimer, *In Proceedings of the Topical Meeting on Photon Correlation Techniques and Applications*, Ed. A. Smartand, J. Abbiss, Optical Society of America, Washington (1988)

[43] B. J. Ackerson,, R.L Dougherty,N.M. Reguigui and U. Nobbmann, J. Thermophys. Heat Transfer 6, 577 (1992)

[44] R.L Dougherty, B. J. Ackerson, N.M. Reguigui, F. Dorr-Nowkoorani and U. Nobbmann, J. Quant. Spectros. Radiat. Transfer 52, 713 (1994)

[45] F.C. Mackintosh and S. John, Phys. Rev. B 40, 2383 (1989)

[46] A. A. Middleton and D. S. Fisher, Phys. Rev. B 43, 5934 (1991)

[47] D.J. Durian,*Two-stream Theory of Diffusing-light Spectroscopies*, Physica A 229, 218 (1996)

[48] W. E. Meador and W. R. Weaver, J. Atmos. Sci., 37630 (1980)

[49] P. D. Kaplan, A. D. Dinsmore, A. G. Yodh and D. J. Pine. Phys. Rev. E 50, 4827 (1994)

[50] D. J. Durian, Phys. Rev. E 51 (1995) 3350

[51] A. M. Wallace, B. Liang, E. Trucco and J. Clark: *Improving Depth Image Acquisition Using Polarized Light*, International Journal of Computer Vision 32, 2, 1 (1999)

[52] J. E Hansen, *Multiple Scattering of Polarized Light in a Planetary Atmosphere*, J. Atmos. Sci. 28, 26,1400 (1971)

[53] B.D. Cameron, M.J. Rakovic, M Mehrubeoglu, , G. Kattawar, S. Rastegar, L.V Wang, and G.L Cote, *Two-Dimensional Mueller Matrix Imaging of Polarized Backscattered Light from a Turbid Medium*, Opt. Lett. 23, 7, 485 (1998)

[54] *Handbook of Optical Biomedical Diagnostics*, Ed. V. V. Tuchin (2002)

[55] B.J. Ackerson, V. Tata, and R.L. Dougherty, *Four-Flux Model for Polarization*, in preparation for submission to the Journal of Quantitative Spectroscopy and Radiative Transfer

[56] A.S.Martinez, Ph.D. dissertation, Fourier University, Grenoble, France (1993)

[57] D. Bicout, C. Brosseau, A.S. Martinez, J.M. Schmitt, *Depolarization of Multiple Scattered Waves by Spherical Diffusers: Influence of the size parameter*, Phys. Rev. E 49, 2 ,1767 (1994)

[58] F. C. Machintosh, J. X. Zhu, D. J. Pine, D. A. Weitz, *Polarization Memory of Multiply Scattered Light*, Phys. Rev. B 40,13, 9342 (1989)

[59] X. Qiu, X. L. Wu, J. Z. Xue, D. J. Pine, D. A. Weitz, and P. M. Chaikin, *HydrodynamicIinteractions in Concentrated Suspensions,* Phys. Rev. Lett. **65**, 516 (1990)

VITA

Zeynep Gunay

Candidate for the Degree of

Master of Science

Thesis: DYNAMIC FOUR-STREAM MODEL FOR POLARIZATION

Major Field: Physics

Biographical:

Personal Data: Born in Ankara, Turkey, on October 5, 1976, the daughter of Yilmaz and Tulin Gunay.

Education: Received Bachelor of Science degree in Physics from Ege University of Izmir, Turkey. Completed the requirements for the Master of Science degree with a major in Physics at Oklahoma State University in December, 2002